Synergistic *MAPT* mutations as a platform to uncover modifiers of tau pathogenesis

Miles R. Bryan III[1,2], Michael F. Almeida[2,3,4], Kyle Pellegrino[1,4], Carli K. Opland[1], Ethan Paulakonis, J.[1] McGillion-Moore[1], Hanna Trzeciakiewicz[1], Diamond King[1], Xu Tian[1], Jui-Heng Tseng[1,2,5], Jonathan C. Schisler[3,4], Nicholas G. Brown[4], Ben A. Bahr[2,6], Todd J. Cohen[1,2*]

[1]Neurology, University of North Carolina- Chapel Hill, NC
[2]Duke-University of North Carolina Alzheimer's Disease Research Center (ADRC), 2424 Erwin Road, Durham, North Carolina 27705
[3]McAllister Heart Institute and the Department of Pharmacology, 111 Mason Farm Road, University of North Carolina - Chapel Hill, Chapel Hill, North Carolina 27514 U.S.A.
[4]Pharmacology, University of North Carolina- Chapel Hill, NC
[5]School of Life Sciences, Arizona State University- Tempe, AZ
[6]Biotechnology Research and Training Center, University of North Carolina- Pembroke, NC

From the Department of Neurology, UNC Neuroscience Center, University of North Carolina, Chapel Hill North Carolina, 27599

*To whom correspondence should be addressed: Todd J. Cohen: Department of Neurology, University of North Carolina at Chapel Hill, Chapel Hill NC 27599
toddcohen@neurology.unc.edu; Tel. (919) 966-3759; Fax. (919) 843-4576

Keywords*:* aggregation, Alzheimer's disease, FTDP-17, MAPT, posttranslational modification (PTM), heat-shock proteins, Hsp70, organotypic brain slices, neurodegeneration, tau, tauopathy

---

Abstract

The natively unfolded tau (MAPT) protein is extremely soluble, which poses challenges when modeling neurofibrillary tangle (NFT) pathology in Alzheimer's disease (AD). To overcome this hurdle, we combined P301L and S320F mutations (PL-SF) to generate a rapid and reliable tau pathology platform to expedite the discovery of factors that modify tau aggregation. Using this model, we evaluated heat-shock proteins (Hsp), which have been linked to tau pathology, but whose role in AD remains enigmatic and controversial. In primary neurons, expression of Hsp70, but not Hsc70 or Hsp90, exacerbated tau aggregation. Conversely, lowering Hsp70 or employing a chaperone-deficient tau mutant (PL-SF-4Δ) reduced tau phosphorylation and abrogated tau aggregation, highlighting Hsp70 as a key driver of tau aggregation. Hsp70 foci clustered within

and surrounding neuritic plaques and NFTs in post-mortem AD brain. Functionally, mature aggregate-bearing neurons showed deficits in neuronal firing and network communication, which were restored by chaperone-binding deficient tau variants that abrogated tau pathology. This study provides a powerful cell-intrinsic model for accelerated tau aggregation, which can be harnessed to identify potent regulators of tau aggregation as promising therapeutic targets.

Introduction

Aggregation of the microtubule-associated protein tau (MAPT) and the formation of insoluble tau inclusion pathology are hallmark features of Alzheimer's disease and related neurodegenerative disorders. In contrast to AD, in which tau pathology is comprised of normal wild-type tau proteins, pathogenic disease-causing mutations in *MAPT* are implicated in familial frontotemporal dementia linked to chromosome 17 (FTDP-17). Over 50 different pathogenic *MAPT* missense, silent, and intronic mutations have been identified[1]. In many instances, missense mutations generate loss and gain of function phenotypes including altered microtubule (MT) binding and enhanced tau aggregation propensity, which are implicated in prion-like tau spreading along defined spatial and temporal brain networks.

While familial missense mutations at residue P301 (e.g., P301L and P301S) have been well characterized as aggregate-prone and MT-binding deficient, less is known about nearby mutations within the MT-binding repeat domain (MTBR). Our recent study characterized a panel of FTDP-17 tau mutations spanning this domain and found that the cellular surveillance machinery composed of HDAC6 and associated chaperones (e.g. Hsp70) shows increased binding to two specific mutations within the R3 domain (P301L and S320F), but not others, suggesting these two

34 mutants are conformationally distinct and are more effectively recognized by the quality control
35 machinery that targets tau for degradation[2].

36 In separate studies, the P301L and S320F mutations were combined into the same full-
37 length tau molecule (termed PL-SF), which generated a surprisingly aggregate-prone
38 conformation leading to an accelerated AD-like tangle pathology, neuroinflammation, and
39 memory impairments in mice and rhesus macaques[3–7]. Thus, PL-SF could potentially be leveraged
40 as an intrinsic, cell-autonomous, and seeding-independent model of full-length tau aggregation,
41 which would otherwise be challenging to achieve with full-length tau. In fact, many widely used
42 tau biosensor models employ artificial, truncated tau mutants comprising only the tau repeat
43 domain, a fragment with questionable physiological relevance to neurons[8]. Once fully
44 characterized, the PL-SF model offers several advantages, including serving as a rapid model of
45 mature tau aggregation and as a cornerstone for high-throughput discovery of tau modifiers.

46 The extent to which tau-bound chaperones such as inducible Hsp70, constitutive Hsc70,
47 and related Hsp90 modulate tau function remains unclear. This debate has obvious therapeutic
48 implications since Hsp inhibitors are in clinical development and have been evaluated in
49 preclinical models of AD[9–14]. However, prior studies have yielded quite contradictory and even
50 opposing results, since on the one hand, Hsp70 facilitates the MC1-positive tau conformation[15],
51 while other studies suggest Hsp70 and Hsc70 mediate tau degradation via autophagy and the
52 ubiquitin-proteasome system (UPS)[16,17]. One possible explanation for these discrepancies is the
53 inability to generate mature tau pathology as observed in human AD brains. Adding additional
54 complexity, tau interacts with dozens of chaperone adaptors and cofactors that may promote or
55 suppress chaperone function directed towards tau[18–21]. Here, we characterized a tau PL-SF model

56 of accelerated tau pathology, which allowed us to interrogate the role of Hsp70 and other
57 chaperones as bona fide modifiers of tau-mediated toxicity and aggregation.
58
59 **Results**
60
61 **Synergistic familial *MAPT* mutations drive tau phosphorylation and aggregation**
62 We first evaluated tau aggregation in PL-SF expressing immortalized QBI-293 cells. Cells
63 transfected with human T40 (2N4R) wild-type, P301L, S320F, or PL-SF were monitored for
64 RIPA-soluble expression of phosphorylated tau (AT8 and AT100) and cleaved tau (TauC3), two
65 well-established markers of tau pathogenesis. Phosphorylated tau accumulated in PL-SF
66 expressing cells, more so than WT or either single mutant (**Figure 1 A, B**). Confirming this finding,
67 total tau immunoblotting revealed up-shifted tau protein bands in SF and PL-SF, indicative of tau
68 hyperphosphorylation. Surprisingly, the single PL mutant appeared hypo-phosphorylated
69 compared to WT or SF mutations. Immunocytochemistry confirmed these findings and revealed
70 Thioflavin S (ThioS) positive SF and PL-SF aggregates, consistent with enhanced tau aggregation
71 (**Supplemental Figure 1, Figure 1C**). Similar to phosphorylated tau, cleaved tau also
72 preferentially accumulated in SF or PL-SF expressing cells.
73 Multiple familial FTD-associated mutations occur at residue P301 (P301L, P301S, P301T)
74 and S320 (S320F, S320Y). We evaluated a panel of other combination mutants by immunoblotting
75 and immunocytochemistry and found that all double mutants formed phosphorylated, cleaved, and
76 insoluble tau species compared to individual single tau mutants (**Supplemental Figure 2**). The
77 most consistently insoluble tau species was PL-SF, which we selected for follow-up analysis.

78 A prior study found that deletion of four key residues in tau (I277/I278 and I308/V309)
79 can abrogate Hsp70 binding[22]. Since the role of Hsp70 in tau pathology is unclear, we generated a
80 PL-SF mutant in which these four residues were depleted, termed PL-SF 4Δ. In transfected QBI-
81 293 cells, PL-SF 4Δ was nearly completely dephosphorylated and accumulated negligible amounts
82 of cleaved tau. PL-SF 4Δ was also downshifted compared to PL-SF (**Figure 1D, E**) and showed
83 significantly less phosphorylated (AT8), cleaved (TauC3), and aggregated (ThioS) tau
84 (**Supplemental Figure 3, Figure 1F**). By co-immunoprecipitation assays, we confirmed that PL-
85 SF 4Δ abrogated the majority of Hsc70 and Hsp70 binding to tau. We did not observe detectable
86 and specific binding to endogenous Hsp90 in our model (**Figure 1G**).
87 We also assessed the impact of tau mutants on acetylated-tubulin (ac-tubulin), a readout
88 for microtubule (MT) stability and dynamics. Wild-type tau increased ac-tubulin, as expected,
89 while P301L or S320F were less effective (~30-40%). Consistent with a near-complete loss of MT
90 regulatory function, PL-SF reduced ac-tubulin levels down to the levels of non-transfected cells.
91 Surprisingly, PL-SF 4Δ partly restored the tubulin interactions (**Figure 1H, I**).
92 To confirm that PL-SF has increased intrinsic propensity to self-aggregate, as opposed to
93 being influenced by other cellular factors, we performed in vitro Thioflavin T (ThioT) assays using
94 recombinant purified tau proteins to assess aggregation kinetics in the presence of heparin as an
95 inducing agent. Indeed, PL-SF tau rapidly aggregated within 1 hr post-induction, at which point
96 the formation of recombinant tau fibrils plateaued, while PL-SF 4Δ was completely resistant to
97 aggregation, even though similar tau concentrations were present (**Figure 1J**).
98
99 **Impaired chaperone binding alleviates tau pathology in neurons**

100 To validate our findings in neurons, we developed mutant tau lentiviral constructs suitable
101 for high-efficiency transduction into mouse primary cortical neurons. Transduced primary
102 neurons were evaluated with a panel of tau mutants, including PL-SF. Immunoblotting of neuronal
103 lysates showed that PL-SF tau was again up-shifted and accumulated more phosphorylated tau
104 (**Figure 2A, B).** Unlike immortalized cell lines, neurons did not show appreciable levels of cleaved
105 tau (TauC3). Only PL-SF accumulated in the insoluble fraction (**Figure 2C**). PL-SF 4Δ showed a
106 marked reduction in tau phosphorylation and aggregation, suggesting a similar phenotype in
107 neurons as well. In fact, deletion of just two of the Hsp-binding residues (ΔI277/I278 or
108 ΔI308/V309) abrogated tau phosphorylation and aggregation, with residues I308/V309 showing
109 the most dominant effect (**Figure 2A-C**). Introduction of β-sheet disrupting proline mutations has
110 been shown to abrogate tau aggregation[23–27]. Indeed, by mutating residues I277 and I308 to
111 prolines (PL-SF I277P/I308P), we were able to suppress tau aggregation to similar levels as seen
112 in PL-SF 4Δ (**Supplemental Figure 4**).

113 By performing microscopy on transduced neurons, we found that PL-SF accumulated AT8,
114 MC1, and ThioS-positive tau inclusions (**Figure 2D, E**). Both MC1 (pre-tangle confirmational
115 tau) and AT8 immunoreactive tau were amorphous and globular and accumulated as large
116 varicosities, or swellings, within neurites. The large globular tau aggregates colocalized with
117 ThioS, supporting tangle-like pathology (**Figure 2F, G**). By transducing neuronal cultures with
118 GFP-tagged PL-SF and labeling neurons with a mouse-specific tau antibody (monoclonal T49),
119 we observed recruitment of endogenous mouse tau to PL-SF inclusions, implying that no species
120 barrier exists between human PL-SF aggregates and mouse tau (**Figure 2H**). PL-SF behaved
121 similarly in tau knockout neurons, and therefore, endogenous tau is not required for the
122 accumulation of PL-SF pathology in neurons (**Supplemental Figure 5**).

123 **Hsp70 promotes tau hyperphosphorylation and aggregation**

124 To determine whether Hsp70 is a more potent regulator of tau pathology compared to other
125 tau-associated heat shock proteins, PL-SF expressing neurons were co-transduced with either
126 HSP70, HSC70, or HSP90. Only Hsp70, but not Hsc70 or Hsp90, exacerbated tau phosphorylation
127 (AT8), which was supported by an appreciable upshift in tau's molecular weight (**Figure 3A, B**)
128 and a trend towards increased levels of total insoluble tau (**Figure 3C, D**). Hsp70 significantly
129 increased AT8, MC1, and ThioS immunoreactivity (**Figure 3E, F**). The effect of Hsp70 appears
130 remarkably specific to the aggregate-prone PL-SF tau, since the P301L single mutant was
131 unaffected **(Supplemental Figure 6).**

132 Next, we depleted HSP70 in PL-SF transduced neurons. We achieved ~ 50% Hsp70
133 knockdown using lentiviral shRNA transduction, which did not affect HSC70 expression.
134 Strikingly, HSP70 knockdown led to ~70% decrease in phosphorylated tau (**Figure 4 A, B**) and
135 ~50% decrease in total insoluble tau (**Figure 4C, D**). We note that a ~50% decrease in soluble tau
136 was also observed, suggesting that Hsp70 depletion enhances the turnover of steady-state tau levels
137 (**Figure 4A, B**). The impact of Hsp70 on tau also appears to be quite specific since knockdown of
138 HSP90 did not alter total or phosphorylated tau (**Supplementary Figure 7**). Overall, our findings
139 highlight Hsp70 as a primary regulator of aggregate-prone tau species in this accelerated PL-SF
140 tau model.

141

142 **Cell-autonomous aggregated tau alters neuronal activity and network synchrony**

143 Given the extensive tau pathology observed in PL-SF transduced neurons, we evaluated
144 any deficits in neuronal activity and connectivity. Electrically active neurons were transduced at
145 DIV18 following an initial multi-electrode array (MEA) recording. Daily recordings were taken

146 for 53 days, and in parallel, neurons were immunolabeled at DIV29 and DIV62 to assess the extent
147 of tau pathology.

148 We evaluated the mean firing rate (a measure of overall activity), the number of network
149 bursts (a measure of neuronal connectivity), and the area under the normalized crossed-correlation
150 (a readout for neuronal synchrony). After 15-20 days post-lentiviral transduction, PL-SF neurons
151 showed a decline in all three metrics, suggesting a loss in neuronal activity and reduced
152 synchronous firing across neuronal networks. The deficits worsened over time, but some neurons
153 continued to fire even past DIV50 (**Figure 5A-C**). Raster plots at DIV54 highlight reduced
154 network firing across electrodes and elongated network firing time (**Figure 5D-F**). PL-SF 4Δ did
155 not exhibit any deficits in any of the activity metrics and showed similar firing patterns as
156 compared to wild-type control neurons (**Figure 5A-C**).

157 The impact of aggregate-prone tau mutants on neuronal firing could represent a direct
158 effect of tau at the synapse. Therefore, we assessed whether PL-SF accumulated at the post-
159 synaptic density (PSD), a re-localization thought to coincide with synaptic dysfunction. PSD
160 fractions were biochemically isolated from transduced neurons at DIV18 and probed by
161 immunoblotting for phosphorylated and total tau. PL-SF accumulated in the PSD fraction, which
162 was not observed with PL-SF 4Δ or any single tau mutants (e.g., P301L) (**Figure 5G**). We
163 conclude that mature PL-SF tau aggregates accumulate at the PSD and drive synaptic dysfunction.
164 By abrogating Hsp binding, PL-SF 4Δ bypasses these defects.

165 PL-SF expressing neurons were aged in culture to determine tau phenotypes over time.
166 Indeed, aged neurons accumulated dense tau inclusions comprised of phosphorylated, MC1, and
167 ThioS-positive tau at DIV29, which became even more intensely labeled by DIV62. All indicators
168 of tau pathology were absent in PL-SF 4Δ expressing neurons, even at late time points (**Figure**

169 **5H**). We also note that Hsp70 began to colocalize with aggregated tau in aged neurons (**Figure**
170 **5I**), supporting aggregation-dependent recruitment of Hsp70.
171
172 **Cell-autonomous tau pathology in organotypic brain slice cultures**
173 To validate our findings in brain culture systems comprised of both neurons and glia, we
174 transduced adult rat organotypic hippocampal brain slices ex vivo with either GFP alone, wild-
175 type tau-GFP, PL-SF-GFP, or PL-SF 4Δ-GFP at DIV1 and imaged brain slices after nine weeks in
176 culture **(Figure 6A, B**). Similar to cultured neurons, PL-SF accumulated dense AT8 and MC1-
177 positive inclusions and distinct neuritic puncta, or foci. Most tau pathology preferentially
178 accumulated in the dentate gyrus (DG) and extended through the hippocampal CA1 and CA3
179 regions. In contrast, PL-SF 4Δ exhibited diffuse, non-aggregated neuronal labeling in the DG and
180 showed far lower levels of pathogenic tau markers, such as MC1 and AT8 **(Figure 6C, D)**. These
181 data suggest that, in a multicellular model with complete hippocampal architecture, abrogating
182 tau-Hsp binding can confer neuroprotection.
183
184 **Hsp70 is upregulated in human AD brain and intercalates within tau aggregates.**
185 Finally, we evaluated Hsp70 levels and localization in AD human post-mortem brain.
186 Biochemical fractionation of control and AD brain lysates showed elevated Hsp70 expression in
187 both soluble (hi-salt extracted) and insoluble (urea extracted) whole cortex AD brain homogenates
188 (**Figure 7A,B**). Hsc70 was only upregulated in the insoluble fraction of AD brains (**Figure 7C,D**).
189 We then performed immunohistochemistry on AD hippocampus and found that the vast majority
190 of AT8-positive tau aggregates (plaques and tangles) were labeled by Hsp70-positive foci (**Figure**
191 **7E, Supplemental Figure 8**). Interestingly, the Hsp70 foci formed discrete puncta that appeared

192 to intercalate within the AT8-positive tau neuritic plaques and neurofibrillary tangles (NFTs). This
193 data further supports a prominent role for Hsp70 in modulating tau accumulation in human AD
194 brain.
195
196 **Discussion**
197 Here, we developed and characterized a cell-autonomous model of tau aggregation based
198 on the synergistic aggregation of tau missense mutations at residues P301 and S320. Given the
199 rapid and robust tau aggregation observed within days (in primary neurons), the PL-SF model
200 readily lends itself to identifying factors that modulate tau aggregation. We leveraged this model
201 to clarify the longstanding debate on the role of Hsp70 as a tau modifier. The PL-SF model could
202 address the stepwise development of tau pathology and provide a more reliable and sensitive
203 system for identifying subtle regulators of tau pathogenesis.
204
205 **Synergistic tau mutants as a model of mature tauopathy**
206 Prior studies have suggested that combining tau mutations at P301 and S320 (e.g. PL-SF)
207 can lead to accelerated tau aggregation[3–6,28], leading to the development of new cell culture and
208 mammalian models that better recapitulate tau pathology. For example, the S320F mutation was
209 introduced in P301S/S305N knock-in mice, resulting in enhanced tau pathology[29]. Recently,
210 AAV-mediated delivery of PL-SF tau to rhesus macaques was able to induce rapid and progressive
211 tau pathology, demonstrating its utility as an efficient primate model for studying AD[30] . Here,
212 we analyzed the biochemical and histological properties of PL-SF in cells, cortical neurons, and
213 organotypic brain slice cultures. Strikingly, PL-SF tau inclusions appear quite similar to those
214 detected in post-mortem AD brain (**Figures 1, 2, 6, 7**). Future cryo-EM studies may be needed to

215 better define their ultrastructural properties[31–34] . However, if PL-SF does indeed form AD-like
216 filaments, it may be a preferred model over other single tau variants (P301S and P301L) that lack
217 mature amyloid structure in culture and mouse models[35,36]. The PL-SF tau variant also
218 accumulated at the post-synaptic density (PSD), leading to functional deficits in neuronal firing
219 and connectivity (**Figure 5 A-H**), which supports its synaptic toxicity. This rapidly maturing
220 pathology likely allows for the rapid occurrence of sensitized functional defects at the synapse and
221 may also affect other cellular processes.

222 Exactly how these two mutations (P301L or S320F) synergize to promote tau pathology
223 and drive tau-mediated toxicity is unclear. But we can envision several scenarios. First, P301L and
224 P301S have been well-characterized for disrupting MT dynamics and promoting tau aggregation;
225 however, less is known about S320F, which is linked to Pick's disease. Recently, S320F was found
226 to stabilize a hydrophobic pocket of tau, exposing the ^{306}VQIVYK^{311} amyloid motif and thereby
227 promoting aggregation[37]. The combination of these two mutations likely amplifies their proclivity
228 towards β-sheet self-assembly. To further test this, we generated PL-SF I277P/I308P containing
229 two amyloid-breaking proline mutations within the MTBR. Indeed, insertion of β-breaking
230 mutations suppressed tau aggregation in primary neurons (**Supplemental Figure 4**), in line with
231 previous in vitro studies[23–27].

232 Second, by extension of its aggregation propensity, PL-SF tau may also be more highly
233 decorated with pathological PTMs than either single tau mutant, driving conformational changes
234 (i.e., MC1). In this study, we only evaluated well-known tau phosphorylation epitopes (AT8,
235 AT100, AT180), but future mass spectrometry approaches could determine the temporal
236 emergence of global tau PTMs (**Figure 2A, B**). For instance, increased PTM complexity could
237 create a feed-forward cycle leading to further loss of tau-MT binding. One can also envision PTM-

238 induced loss of tau binding to quality control machinery, which typically acts in a compensatory
239 manner to prevent aberrant tau[2]. One example is the surveillance factor HDAC6, which binds and
240 maintains tau in the deacetylated state[2]. Thus, PL-SF could overburden the cellular proteostasis
241 capacity, as suggested for human AD[38–40].

242 Third, P301L and S320F mutations are also known to dissociate tau from microtubules,
243 which would shift and favor their equilibrium, further concentrating tau pools in the cytosol and
244 facilitating their aggregation. PL-SF drastically reduced acetylated-tubulin levels back down to
245 baseline (i.e., non-tau expressing cells) (**Figure 1 H, I**), suggesting PL-SF is almost completely
246 disassociated from microtubules and therefore more readily primed for aggregation.

247 Lastly, once formed, we found that neuronal PL-SF tau can recruit endogenous mouse tau
248 (detected by T49 antibody) into tau inclusions (**Figure 2H**), consistent with a prior study showing
249 that human PL-SF-expressing mice (SPAM mice) recruited endogenous mouse tau[6,28]. PL-SF tau,
250 therefore, may be more highly seeding competent, in a species-independent manner, which could
251 be leveraged to model tau spreading since it poses several advantages over the use of exogenously
252 added, brain-derived AD seeds (e.g., large-scale production, reliability and reproducibility, and
253 fully intact N-terminal domains). We reiterate that further ultrastructural studies are needed to
254 determine whether seeding-competent PL-SF resembles human AD brain-derived tau.

255

256 **The role of Hsp70 in tau pathology**

257 We added clarity to the long-standing question of whether Hsp70 modulates tau
258 aggregation, as the prior literature is inconsistent and often highlights contradictory models for tau
259 triage via coordinated Hsp binding. Some studies have found that activation or overexpression of
260 Hsp70 can suppress tau aggregation in vitro, which would intuitively suggest a classical Hsp70

261 chaperone activity as a suppressor of tau aggregation[16,17,41,42] . Adding additional complexity,
262 while Hsp70 can disassemble tau filaments isolated from human AD brain, this chaperone activity
263 can release seeding-competent tau species, suggesting any protection afforded by Hsp70 may
264 depend on the nature of the chaperone-liberated tau species[43]. In contrast, other studies have shown
265 that Hsp70 depletion or small molecule inhibition (YM-01, JG-23/48) may drive tau
266 clearance[11,13,44–48]. We sought to reconcile these differences in the context of our PL-SF cellular
267 model of tau aggregation.

268 We initially found that Hsp70 was tightly associated with PL-SF tau aggregates in vitro
269 and in cell culture, a finding consistent with a previous study[49] (**Figure 5I**). HSP70 overexpression
270 was associated with PL-SF phosphorylation and aggregation, while HSP70 depletion reduced total
271 tau levels, including hyperphosphorylated and aggregated tau species (**Figure 3A-D, Figure 4A-**
272 **D**). Furthermore, abrogating Hsp70 binding using an Hsp70-binding deficient mutant (PL-SF-4Δ)
273 was also sufficient to suppress tau aggregation (**Figure 1, 2, 5, 6)**. Further supporting a role for
274 Hsp70 in human AD pathology, we found that Hsp70 is upregulated in AD hippocampus and
275 heavily intercalated within neuritic plaques and NFTs (**Figure 7**). The Hsp70 localization pattern
276 was highly consistent in human AD hippocampus (**Supplemental Figure 8**) and illustrates a
277 unique tau-Hsp70 pattern of co-pathology[50–52]. The lack of complete colocalization suggests that
278 Hsp70 recruitment to tau occurs in a time-dependent manner. At least in a mature tau aggregation
279 model, these data are consistent with Hsp70 stabilizing a misfolded tau conformation that
280 potentially evades proper triage and/or degradation.

281 In addition to Hsp70, tau is also an Hsp90 substrate, which competes for binding sites
282 within tau's MTBR and is thought to promote CHIP-mediated tau degradation and clearance[21,53–
283 59]. It is plausible that aggregated tau may form as a consequence of an imbalance in the ratio of

284 Hsp70 vs. Hsp90 binding, which, if shifted towards Hsp70, could radically shift tau processing
285 away from degradation towards stabilization of aggregated tau intermediates. In this scenario,
286 Hsp70 depletion or inhibition would facilitate proteasome or autophagic targeting (degradation)
287 by shifting the balance away from tau refolding. Future proteomics studies will be needed to
288 determine whether distinct tau triage complexes emerge temporally in response to tau aggregation.
289 For example, identifying the PL-SF interactome over time may reveal distinct triage stages in
290 which Hsp70 has shifted from pro-folding to pro-aggregation[60].

291 We did not observe any effect of Hsc70 on tau aggregation. Though highly homologous,
292 Hsc70 is constitutively expressed at ~30-fold higher levels in the brain compared to the inducible
293 Hsp70 isoform[61]. Hsp70, but not Hsc70, overexpression increased the number of MC1-positive
294 neurons by nearly 3-fold (**Figure 3E, F**). Since Hsp70 is more sensitive to redox signaling (via
295 cysteine residue reactivity), its activity towards tau may be more tunable under stress conditions[62].

296 Prior work has shown that the functional outcome of Hsp70-tau interactions is highly
297 dependent on the specificity and fine-tuning provided by co-chaperones that regulate Hsc70[19],
298 Hsp90[63–65] , CHIP[61] , as well as small heat shock proteins[66–68]. Thus, we suspect that many
299 variables could dictate how effectively and efficiently Hsp70 targets tau, including: 1) the extent
300 of MT-dissociated aggregated tau present, 2) the relative balance and abundance of chaperones,
301 co-chaperones, and cofactors that target and triage tau, and 3) the notion that disease onset and
302 disease progression (either acute or chronic) may involve distinct signaling pathways or
303 compensatory responses.

304 Taken together, our study supports the notion that depletion or activity-modifying
305 approaches targeting Hsp70 (or its cofactors and co-chaperones) may be neuroprotective in the
306 context of the AD brain. While brain-specific HSP70 knockout mice are not available (to the best

307 of our knowledge), brain-permeable Hsp70 inhibitors may have therapeutic utility, although broad
308 Hsp70 inhibition could have detrimental effects on overall brain proteostasis. Therapeutic
309 strategies aimed at "precision proteostasis" could selectively modulate chaperone–client
310 interactions to favor the clearance of pathogenic tau without compromising global protein
311 homeostasis and without directly targeting tau itself.
312

313 **Materials and Methods**

314

315 **Plasmid and lentivirus cloning**

316 To generate the pUltra-T40 WT, PL, PL-SF, SF, PL/SF-2Δ (277-278), PL/SF-2Δ (308-309),
317 PL/SF-4Δ, HSC70-flag, HSP70-flag, and HSP90-flag constructs, the cDNAs were amplified
318 through PCR and inserted into the pUltra vector using AgeI and SalI restriction endonucleases to
319 replace eGFP in pUltra. pUltra-XeGFP was made by removing eGFP using AgeI and BspEI,
320 creating a blunt end with Klenow before circularizing. pUltra-T40 WT (eGFP), PL/SF (eGFP),
321 and PL/SF-4Δ (eGFP) were created by replacing TDP43 in pUltra TDP43 WT (eGFP) using BspEI
322 and SalI. To generate PL/SF/2IP, two consecutive Q5 site-directed mutagenesis were performed
323 on PL/SF(eGFP). pUltra was ordered from Addgene (Plasmid #24129). pUltra was a gift from
324 Malcolm Moore (Addgene plasmid # 24129; RRID:Addgene_24129). shRNA plasmids against
325 HSP70 (TRCN0000098597, TRCN0000098598) and HSP90 (TRCN0000008491,
326 TRCN0000008494) were ordered from the UNC Lenti-shRNA Core Facility. Primers used for
327 vector construction are in Table 1.
328

329 **QBI-293 cell culture**

330 QBI-293 (HEK293A) cells (ThermoFisher, #R70507) are commercially available and maintained
331 according to standard protocols. QBI-293 cells were cultured in complete DMEM media (10%
332 fetal bovine serum, 1X L-glutamine, and 1X penicillin/streptomycin). QBI-293 cells were
333 transfected with FuGENE 6 transfection reagent (Promega) to express 2N4R tau constructs for 48
334 hr. Following transfection, cells were lysed and collected in 1X RIPA buffer [50 mM Tris pH 8.0,
335 150 mM NaCl, 5 mM EDTA, 0.5% sodium deoxycholate, 1% Igepal CA-630, 0.1% SDS]
336 supplemented with deacetylase, phosphatase and protease inhibitors: 1 mM phenylmethylsulfonyl
337 fluoride (PMSF), 10 mM Nicotinamide (NCA), 1 mM sodium orthovanadate (Na3VO4), 1 mM
338 sodium fluoride (NaF), 0.5 M β-glycerophosphate, 2 μM Trichostatin A (TSA), and protease
339 inhibitor cocktail composed of L-1-tosylamide-2-phenylethylchloromethyl, N-tosyl-L-lysine
340 chloromethyl ketone, leupeptin, pepstatin, and soybean trypsin inhibitor, each at 1 μg/ml.
341

342 **Primary cortical neuron cell culture**

343 Mouse primary cortical culture was performed in accordance with the University of North Carolina
344 (UNC) Institutional Animal Care and Use Committee (UNC IACUC protocol 24-190). Mouse
345 cortical neurons were dissected and isolated from C57Bl/6 mice (Charles River) at embryonic day
346 15-16 following lethal isoflurane anesthesia. Following anesthesia, embryos were removed from
347 the pregnant abdominal cavity, washed well with ice-cold 70% ethanol and placed in cold Hanks-
348 buffered balanced salt solution (HBSS). Once rinsed, these embryos were moved to a 10cm dish
349 for dissection. The embryos were then removed from the placental membrane and brains were
350 isolated. The cortex was dissected then moved to Hibernate-E solution (BrainBits) with B27
351 (Gibco) and Glutamax (ThermoFisher). The cerebral cortices were minced thoroughly with
352 forceps and incubated for 30 minutes at 37 °C in HBSS with 20 U/mL papain (Worthington

353 Biomedical), 1mM EDTA, 0.2 mg/mL L-Cysteine, and 5U/mL DNAse (Promega). Cortical tissue
354 was further dissociated in plating media (BrainPhys media (Stemcell), 5% fetal bovine serum, 1X
355 B27 (Gibco), 1X penicillin/streptomycin (Gibco), and 1X Glutamax by triturating the sample using
356 a P1000 micropipette. This suspension was centrifuged for 5 minutes at 1.5 rcf to pellet the cells.
357 The pellet was then resuspended in plating media and passed through a 40 μm cell strainer. A
358 Countess 3 automated cell counter (Invitrogen) was used to count the cells. Cells were plated in
359 plating media at 600,000 cells/well in 6-well plates or 30,000 cells/well in 96-well plates. The next
360 day (DIV1), plating media was completely aspirated and replaced with fresh neuronal media
361 (BrainPhys media (Stemcell), B27 (Gibco), 1X penicillin/streptomycin (Gibco), and 1X
362 Glutamax).
363

364 **Lentiviral production**

365 Lentiviral production was performed by co-transfecting 37.5 mg lentivirus plasmid with 25 mg
366 psPAX2, 12.5 mg VSVG, and 6.25 mg REV plasmids per 15 cm culture plates of Lenti-X 293 T
367 cells (Takara). For each lentiviral construct, three 15 cm plates were used for production. Roughly
368 48 hrs after the transfection, cell culture media was collected and subsequently centrifuged at
369 2000 rcf for 10 minutes. Lentiviral particles were purified using a double-sucrose gradient method
370 as follows: supernatants were loaded onto a 70–60% to 30–20% sucrose gradient and centrifuged
371 at 70,000 rcf for 2 hr at 17 °C. The 30–60% fraction containing the viral particles was retrieved,
372 resuspended in PBS, filtered with a 0.45 mm filter flask, loaded onto a 20% sucrose solution, and
373 centrifuged a second time at 70,000 rcf for 2 hr at 17 °C. The supernatants were carefully
374 discarded, and the viral particles in the pellet were resuspended in PBS, aliquoted and stored at
375 − 80 °C.

376

377 **Lentiviral transductions**

378 Primary neurons were transduced with ~3.0×10^{12} viral particles per mL at DIV4 for most
379 experiments (viruses were added at DIV18 for MEA experiments). If neurons were co-transduced
380 with two viruses, both were added sequentially (each at ~3.0×10^{12} viral particles per mL). For
381 transductions, viruses were added directly to the media in each well (1 µl virus per 2 mL media),
382 followed by gentle rocking by hand to distribute viral particles. The following day, virus-
383 containing media was completely aspirated and replaced with half conditioned media (neuronal
384 media from the same neuron culture) and half fresh neuronal media (BrainPhys (StemCell) with
385 B27 (Gibco), Pen-strep (Gibco), and Glutamax (Gibco)). Every two-three days, half of the
386 neuronal media was discarded and replenished with fresh neuronal media until neurons were
387 collected. Most neurons were collected at DIV10 (7 days after transduction), unless otherwise
388 noted.

389

390 **Immunoblotting and biochemical analysis**

391 RIPA soluble lysates (250 µl per well of a 6-well plate) collected from QBI-293 and primary
392 cortical neuron were sonicated 20 times on ice, then centrifuged at 15,000 rcf for 20 minutes at
393 4 °C. The supernatant was removed from the pelleted material, leaving behind a RIPA insoluble
394 pellet. The RIPA insoluble pellet was washed with 250 µl of RIPA lysis buffer with protease,
395 phosphatase, and deacetylase inhibitors and centrifuged at 15,000 rcf for 20 minutes at 4 °C. This
396 supernatant was removed and discarded and 75 µl of 1% SDS was added to each pellet then
397 sonicated 20 times at room temperature. These samples were then centrifuged at 15,000 rcf at room
398 temperature. The supernatant from these tubes was removed and stored in separate tubes as the

399 SDS-soluble fraction. The RIPA and SDS-soluble supernatants were then mixed with 6X loading
400 dye with DTT and boiled at 98 °C for 10 minutes in a PCR thermocycler (BioRad). Samples were
401 run and resolved via SDS-PAGE on 4–20% gradient gels (BioRad). Gels were transferred to iBlot
402 2 Midi nitrocellulose membranes using the iBlot 2 (Invitrogen) following the standard P0, 7-
403 minute settings. Following transfer, membranes were blocked with 2% milk in 1X TBS for 30
404 minutes and then incubated with primary antibody overnight at 4 °C on a rocker. The next day,
405 membranes were incubated with HRP-conjugated anti-mouse or anti-rabbit antibodies (1:1000)
406 for 1-2 hr at room temperature. Blots were developed with ECL Western Blotting substrate
407 (Cytiva, Amsterdam) and imaged on a GE ImageQuant LAS4000.
408
409 **Immunocytochemistry**
410 Immunocytochemistry experiments were performed using QBI-293 cells or cortical primary
411 neurons plated on poly-D-lysine (PDL)-coated 96-well plates. Following either plasmid
412 transfection (48 hr) or lentiviral transduction (7 days unless otherwise stated), cells were washed
413 once in PBS, immediately fixed in 4% paraformaldehyde for 15 minutes, then washed once more
414 with PBS. Following fixation, cells were then permeabilized with permeabilization buffer (0.2%
415 Triton X-100 (Sigma) in PBS) for 20 minutes then blocking buffer (4% normal goat serum in PBS
416 with 0.05% Tween 20) for 1 hr. Primary antibodies were added in blocking buffer and incubated
417 overnight on a rocker at 4 °C. The following day, cells were washed 3X in PBS with 0.05% tween
418 20 and incubated with Alexa 488, Alexa 594, or Alexa 647 conjugated secondary antibodies at
419 1:1000 and DAPI for 1 hr. Cells were then washed 3X in PBS with 0.05% Tween 20. Cells were
420 then imaged using an EVOS M7000 automated microscope with EVOS 20X objective (Invitrogen
421 AMEP4982) and 40X objectives (Invitrogen AMEP4754) and DAPI, GFP, Texas Red, and Cy5

422 light cubes. Note: Some representative images were artificially brightened or contrasted in
423 Microsoft PowerPoint or Celleste 5.0 and 6.0 software (Invitrogen) to aid visualization. Any panels
424 assessing the same set of conditions were brightened to identical levels. Images were not
425 manipulated prior to quantification.
426
427 **Antibodies**
428 The following primary antibodies were used in this study: AT8 (ThermoFisher Scientific-
429 MN1020), AT100 (ThermoFisher Scientific MN1060), AT180 (ThermoFisher Scientific
430 MN1040), TauC3 (ThermoFisher Scientific-AHB0061), T49 mouse tau (Millipore- MABN827),
431 Tau12 (Millipore, MAB2241, 1:1000), Tau5 (AHB0042), Hsp70 used for immunoblotting (Enzo-
432 ADI-SPA-810-D), Hsp70 used for immunoblotting and immunocytochemistry (Cell Signaling
433 Technologies- 4872), Hsc70 1B5 (ADI-SPA-815-F), Hsp90 16F1 (Enzo- adi-spa-835), Total tau
434 rabbit polyclonal- formerly K9JA (DAKO, A0024 1:2000), GAPDH 6C5 (Millipore- MAB374),
435 ac-tubulin (Sigma T7451), alpha tubulin (Sigma, T9026), Anti-FLAG M2 (Sigma, F1804, 1:2000),
436 GFAP (Dako, 20334). The MC1 antibody was kindly shared by Dr. Peter Davies. Quantification
437 of immunoblotting was measured by ImageStudio Lite Version 5.2.
438
439 **Co-immunoprecipitation reactions**
440 All co-immunoprecipitations were performed in QBI-293 cells transfected with plasmids
441 expressing 2N4R wild-type, P301L, P301L/S320F, and P301L/S320F 4Δ for 48 hrs prior to
442 collection. Each well of a 6-well plate was used as separate conditions. Cells were collected in 250
443 µl RIPA buffer with protease, phosphatase, and deacetylase inhibitors prior to co-
444 immunoprecipitation. Lysates were immediately rotated on a wheel for 30 minutes at 20 rpm at 4

445 ºC. Lysates were then centrifuged at 15,000 rcf for 15 minutes at 4 ºC. Supernatants were removed
446 and 40 µl were kept as input. The remaining supernatant was pre-cleared with 50 µl of Protein
447 A/G PLUS-Agarose beads (Santa Cruz, sc2003) for 30 minutes at 4 ºC. Lysates were centrifuged
448 for 1 minute at 1,500 rcf, and the supernatant was removed. The volume of each reaction was
449 brought to 500 µl of RIPA buffer with inhibitors. For each reaction, 8 µl of tau5 antibody was
450 added to each reaction, then 75 µl of agarose protein A/G beads. Lysates were rotated on a wheel
451 at 20 rpm at 4 ºC overnight. The following day, lysates were centrifuged at 1,500 rcf for 5 minutes.
452 Most of the supernatant was carefully removed, followed by washing with 500 µl of RIPA buffer
453 with inhibitors, and lysates were centrifuged at 1,500 rcf for 5 minutes. This wash was repeated
454 four times. After the final wash, loading dye with DTT was directly added to the beads and heated
455 for 10 minutes at 98 ºC with intermittent mixing. These were centrifuged for 30 seconds at 1,500
456 rcf prior to storage at -80 ºC.
457
458 **Purification of recombinant tau**
459 Tau purification methods were adapted from Barghorn et al, 2004[69]. Untagged wild-type and
460 mutant versions of tau were cloned into pRK172 backbone and transformed into BL21(DE3)-RIL
461 cells. Cells were grown in LB media at 37 °C until the OD600 reached 0.8. Protein expression was
462 then induced with IPTG and continued shaking at 37 °C for 3-5 hrs. After the cells were harvested
463 and resuspended in lysis buffer (20 mM MES pH 6.8, 1 mM EDTA, 5 mM DTT, protease
464 inhibitors benzamidine and leupeptin, and PMSF), the cells were lysed via sonication. Lysed cells
465 were heat shocked at 80 °C for 20 minutes, then centrifuged at 17,500 rpm (36,635 xg) for 30
466 minutes to remove cell debris. Clarified lysate was dialyzed overnight at 4 °C into wash buffer (20
467 mM MES pH 6.8, 50 mM NaCl, 1 mM EDTA, 1 mM $MgCl_2$, 2 mM DTT). Following overnight

468 dialysis, lysates were centrifuged at 17,500 rpm (36,635 xg) for 30 minutes to remove precipitated
469 proteins and then subjected to cation exchange chromatography. The protein was eluted by
470 increasing salt concentration in buffer to 250 mM. The samples were further purified via size
471 exclusion chromatography on a Superdex 200 Increase 10/300 GL column in sizing buffer (25 mM
472 HEPES pH 7.5, 100 mM NaCl, 5 mM $MgCl_2$, 1 mM DTT). Samples were then concentrated as
473 needed using centrifugal filters and flash frozen for later use.
474
475 **Heparin-induced tau aggregation assays:**
476 Tau aggregation assays were carried out in a PolarStar Omega microplate reader using Thioflavin
477 T (ThT) fluorescence to monitor formation of tau aggregates. Aggregation reactions were started
478 by combining 5 μM tau, 2 μM heparin, and 20 μM ThT in reaction buffer (1x PBS, 2 mM TCEP)
479 and transferred to a costar 96-well half-area microplate (black polystyrene, flat bottom, non-
480 treated). The microplate was covered with an ELISA plate sealer and placed in the microplate
481 reader at 37 °C. Fluorescence measurements were taken every 5 minutes for 12 hrs using a 440-
482 10 nm excitation and 485-12 nm emission filter.
483
484 **HSP70 and HSP90 shRNA knockdown**
485 All shRNAs were obtained from UNC Lenti-shRNA core facility and cloned into the pUltra
486 vectors. Sequences: HSP70 shRNA: GCAGGTGAACTACAAGGGCGA; eGFP control shRNA:
487 TACAACAGCCACAACGTCTAT (Y145 to Y151 residues of eGFP). HSP70 shRNAs were
488 added to the neuron culture four days after transduction with tau lentiviruses at a titer of ~3.0×10^{12}
489 viral particles per mL. Media was half exchanged for fresh neuronal media every two days. After
490 an additional four days in culture, primary neurons lysates were collected for experiments. We

491 noted some toxicity after more than 4 days in culture with HSP70 shRNAs. HSP90 shRNAs were
492 applied for 7 days in culture (~3.0×10^{12} viral particles per mL) prior to collection for experiments
493 and were not overtly toxic.

494 **Multi-electrode array recordings and analysis**

495 Following dissection, primary mouse cortical neurons were directly plated onto poly-D lysine
496 coated 24-well BioCircuit MEA plates (Axion Biosystems). A 10 µl droplet of neurons at a
497 concentration of 16,000,0000 neurons/mL was added directly to the center of each well. Neurons
498 were incubated at 37 °C for 1 hr then 250 µl of plating media (BrainPhys media (Stemcell), 5%
499 fetal bovine serum, 1X B27 (Gibco), 1X penicillin/streptomycin (Gibco), and 1X Glutamax) was
500 carefully added to each well in a circular motion. Following another 1-hr incubation, another 250
501 µl of plating media was added to each well (total volume = 500 µl). The following day, ~90% of
502 plating media was aspirated and fresh neuronal (BrainPhys media (Stemcell), B27 (Gibco), 1X
503 penicillin/streptomycin (Gibco), and 1X Glutamax) media was added to each well. Half of the
504 media was exchanged for fresh neuronal media every two days. At DIV18, neurons underwent an
505 initial, 10-minute pre-recording using the Axion Maestro Edge (Axion Biosystems) and AxIS
506 Navigator software (Axion Biosystems). Immediately following this recording, neurons were
507 transduced with lentiviruses at ~3.0×10^{12} viral particles per mL (four replicate wells per condition).
508 The following day, neuronal activity was recorded for 10 minutes, then lentivirus-containing
509 neuronal media was completely replaced with half fresh neuronal media and half conditioned
510 neuronal media from the same culture. Neurons were recorded nearly every day for 10 minutes
511 and half of the neuronal media was replaced every 2-3 days after recording until DIV71 (day 53
512 of recording). Post-hoc analysis was performed using the NeuralMetricTool (Axion Biosystems)
513 using default analysis options. Data was exported into Microsoft Excel, then graphed via GraphPad

514 Prism 10 for statistical analyses and graphing. Raster plots were generated from the same data
515 using the AxIS Metric Plotting Tool. 96 well plates were plated at the same time using the same
516 primary neurons, underwent identical media changes, and were used for immunocytochemistry at
517 DIV29 and DIV62 in Figure 5.
518
519 **Post-synaptic density isolation**
520 Primary mouse cortical neurons from wild-type C57/BL6 mice were plated on poly-D-lysine
521 coated 6-well plates at 600,000 cells/well. Neurons were treated with lentivirus at DIV4 (1 6-well
522 plate per condition) and half-fed every two days until DIV14. At DIV14, neurons were rinsed in
523 cold PBS and all 6-wells of each plate were collected in a total of 900 µl of homogenization buffer
524 (320 mM sucrose, 5 mM sodium pyrophosphate, 1 mM EDTA, 10 mM HEPES pH 7.4) with
525 protease/phosphatase inhibitor cocktail 200 nM okadaic acid, 1 mM orthovanadate, 1X protease
526 inhibitor cocktail (Roche). Neuronal lysates were homogenized by passing the lysate 12 times
527 using a 26g needle. For each condition, 70 µl of lysate was kept and stored as whole cell lysate.
528 The remaining lysate was centrifuged at 1,000 g for 10 minutes at 4 °C *to* generate pelleted nuclear
529 fraction (P1) and supernatant fraction (S1). The S1 fraction was centrifuged at 15,000 g for 20
530 minutes at 4 °C to generate the membrane/crude synaptosome pelleted fraction (P2) and cytosolic
531 supernatant fraction (S2). The P2 fraction was resuspended in 500 µl of ultrapure H_20 with
532 protease/phosphatase cocktail. 20 µl of 100 mM HEPES was added to the 500 µl of suspension to
533 yield 4 mM HEPES pH 7.4. These samples were then spun on a wheel for 30 minutes at 4°C then
534 centrifuged for 20 minutes at 4 °C at 25,000 g using a Sorvall mTX 150 ultracentrifuge (Thermo
535 Scientific) to generate pelleted synaptic fraction (LP1) and supernatant fraction (LS2). The LP1
536 pellet was resuspended in 250 µl mM HEPES pH7.4 using repeated trituration with a micropipette.

537 This was then mixed with 250 µl of 1% Triton X-100 with protease/phosphatase cocktail and spun
538 on a wheel for 10 minutes at 4 °C. This was then centrifuged in Sorvall mTX 150 ultracentrifuge
539 (Thermo Scientific) at 32,000 g for 20 minutes at 4 °C. This pellet was resuspended in 80 µL of
540 50 mM HEPES pH7.4 using micropipette trituration to yield the PSD fraction. Only total
541 homogenate and PSD fraction were processed and analyzed by SDS-PAGE.
542
543 **Imaging quantification**
544 All immunocytochemistry (aside from organotypic slice cultures) quantification was performed
545 using Celleste 5.0 and 6.0 software (Invitrogen). The number of inclusions were counted using the
546 count/size function. Puncta and inclusions were manually segmented based on intensity (Segment:
547 Manual) and size (Region: Area) thresholds for each tau probe (e.g. AT8, MC1, ThioS). These
548 threshold settings were then applied to all images used for that specific experiment, automatically
549 batched processed using a segment-count-export macro generated in Celleste, then exported to
550 Microsoft Excel for subsequent analysis.
551
552
553 **Hippocampal slice cultures**
554 Sprague-Dawley rats (Charles River Laboratories, Wilmington, MA) were housed and maintained
555 in accordance with the recommendations from the Guide for the Care and Use of Laboratory
556 Animals from the National Institutes of Health, and in accordance with an approved protocol from
557 the Institutional Animal Care and Use Committee of the University of North Carolina-Pembroke.
558 Brain tissue from postnatal 12-day-old rats was rapidly prepared and hippocampi positioned on a
559 McIlwain tissue chopper for assembling slices for interface cultures as previously described[70,71].
560 Three-dimensional organotypic cultures of specific brain regions are well known for studying

561 different types of physiologies and pathogenic processes[72–74]. Transverse hippocampal slices (400-
562 µm thickness) were immediately placed in ice-cooled-buffer solution (pH 7.2) then transferred in
563 groups of eight to nine onto the Biopore membrane of culture inserts (Millipore, Billerica, MA).
564 The media below the culture inserts contained 50% basal medium eagle (Sigma-Aldrich, St. Louis,
565 MO), 25% Earle's balanced salts (Sigma-Aldrich), 25% horse serum (Gemini Bio-Products,
566 Sacramento, CA), and defined supplements as previously described[75] . The media were initially
567 changed 24 hrs after the slicing procedure, followed by subsequent changes every 3-4 days. The
568 cultivated hippocampal slices were maintained under conditions of a 5% CO2-enriched
569 atmosphere at a constant temperature of 37 °C for a duration of nine weeks.

570 **Lentiviral infection of organotypic cultures**

571 Lentiviruses expressing GFP or GFP-tagged tau variants (wild-type, PL-SF, and PL-SF 4Δ tau).
572 For each condition, 1.5 µl of lentivirus were applied onto the surface of individual organotypic
573 slices (~7.5×10^{12} viral particles per slice) approximately 3 hrs after the placement of the slices on
574 Millipore inserts. Following a nine-week incubation period in vitro, both the infected organotypic
575 slices and their corresponding controls were fixed with 4% PFA for 3-4 hrs. Subsequently, the
576 slices were rinsed multiple times with PBS and stored in PBS at 4 ºC.

577

578 **Immunofluorescence staining and imaging of organotypic brain slice cultures**

579 The fixed organotypic hippocampal explants underwent permeabilization in PBS containing 0.5%
580 Triton-X100 for 30 minutes. Following this, the slices were blocked with a solution of 5% BSA in
581 PBS containing 0.1% Triton-X100 for 90 minutes at room temperature. Subsequently, the
582 organotypic slices were incubated for 48 hrs at 4 ºC with primary antibodies targeting AT8 (1/400;
583 ThermoFisher Scientific- MN1020) or MC1 (1/400; Dr. Peter Davies, diluted in a solution of 3%

584 BSA containing 0.1% Triton-X100. Next, brain explants were washed 3-4 times with PBS
585 containing 0.1% Triton-X100 and then exposed to Goat anti-mouse IgG Alexa-FluorTM 568
586 (ThermoFisher, Waltham, MA) for 120 minutes at room temperature. Following this incubation,
587 the organotypic slices were rinsed three times with PBS containing 0.1% Triton-X100. During the
588 second wash, NucBlue stain (Invitrogen, MA, USA) was introduced to the PBS to promote DAPI
589 nuclear staining. Subsequently, the slices were rinsed in PBS and were mounted onto glass slides,
590 covered by 1.5 mm coverslips, using ProlongTM diamond antifade mountant (Thermo Fisher
591 Scientific, NC, USA). Immunofluorescence images were captured with Andor Dragonfly spinning
592 disk confocal using the Zyla Plus 4.2MP sCMOS (Oxford Instruments, Abingdon, United
593 Kingdom). Image our blinded processed adopting the equal adjust using the Imaris
594 Multidimensional visualization and analysis software (Schlieren-Zurich, Switzerland).
595

596 **Human brain fractionation**

597 Human control and Alzheimer's disease (AD) cortical brain tissues (Braak stages V–VI) were
598 obtained from the Center for Neurodegenerative Disease Research brain bank at the University of
599 Pennsylvania. Gray matter from the frontal cortex of each subject was isolated and homogenized
600 in 3 volumes per gram (vol/g) of cold high-salt RAB buffer (0.75 M NaCl, 100 mM Tris, 1 mM
601 EGTA, 0.5 mM $MgSO_4$, 0.02 M NaF, 2 mM DTT, pH 7.4), supplemented with deacetylase,
602 phosphatase, and protease inhibitors as previously described. Homogenates were incubated at 4 °C
603 for 20 minutes to facilitate microtubule depolymerization, followed by ultracentrifugation at
604 100,000 × g for 30 minutes at 4 °C. The resulting supernatant was designated the high-salt fraction.
605 The pellet was then re-homogenized and subjected to a second round of centrifugation under
606 identical buffer and conditions. After removal of the supernatant, the remaining pellets were

607 homogenized in 5 vol/g of cold RIPA buffer (50 mM Tris, pH 8.0, 150 mM NaCl, 1% NP-40, 5
608 mM EDTA, 0.5% sodium deoxycholate, 0.1% SDS), and centrifuged once more at 100,000 × g
609 for 30 minutes at 4 °C. Subsequent to myelin flotation, the pellets were re-extracted in RIPA buffer
610 containing 20% sucrose to eliminate residual myelin and labeled as the RIPA fraction. Finally, the
611 insoluble material was extracted using 1 vol/g of urea extraction buffer (7 M urea, 2 M thiourea,
612 4% CHAPS, 30 mM Tris, pH 8.5). Both the high-salt and urea-soluble fractions were subjected to
613 SDS-PAGE followed by immunoblotting with antibodies targeting Hsp70, Hsc70, and GAPDH.
614

615 **Human brain immunohistochemistry and confocal microscopy**

616 Human hippocampal tissue sections mounted on coverslips were obtained from the UNC
617 Translational Pathology Laboratory (TPL), which oversees a cataloged and archived repository of
618 Alzheimer's disease (AD) brain specimens, including neuropathologically confirmed cases from
619 UNC-affiliated donors. The 10 um sections were de-paraffinized with two 45-minute washes in
620 xylene followed by one-minute washes in 100% ethanol (x2), 95% ethanol, 80% ethanol, 75%
621 ethanol, water, and finally allowed to soak O/N in 1x PBS. Antigen retrieval is performed using a
622 citrate-based antigen unmasking solution (Vector Labs, H-3300-250) in boiling Mill-Q water for
623 10-minutes. The slides were then washed 3x5-min with TBS, followed by 1x wash in TBS + 0.1%
624 TritonX-100 for 20 minutes, 3x5-min with TBS, and 1x5 min in 3% Goat Serum in TBS (Southern
625 Biotech, 0060-01). Sections were then stained 2x O/N in a humidified chamber at room
626 temperature using anti-AT8 (1:500, Invitrogen, MN1020) and anti-Hsp70 (1:500, Abcam,
627 ab181606). Slides were then washed 3x5-min with TBS followed by secondary staining with goat
628 anti-mouse IgG 488 (1:1000, Invitrogen, A-11001) and goat anti-rabbit IgG 594 (1:1000,
629 Invitrogen, A-11012) for 24 hours at 4°C in a dark, humidified chamber. Slides were then washed

630 3x5-min with TBS, allowed to dry, and mounted with Fluoromount-G with DAPI (Invitrogen, 00-
631 4959-52).
632 Confocal microscopy was performed on an LSM980 (Zeiss) inverted laser scanning confocal
633 microscope. The LSM980 is equipped with a motorized X, Y, stage and Z-focus with high-speed
634 Piezo insert along with four diode lasers (405, 488, 561, and 633). Images were acquired with 1x
635 Nyquist sampling using 63x 1.4 NA Plan-Apochromat oil objective (Zeiss) and 4 channel GaAsP
636 detectors on Zen Blue 3.6 software. Images were acquired with 1x Nyquist sampling using 20x
637 0.8 NA Plan-Apochromat air objective (Zeiss) and 4 channel GaAsP detectors on Zen Blue 3.6
638 software.
639
640 **Statistical analysis**
641 GraphPad Prism 10 software was used for all statistical analyses. For comparisons between two
642 groups, two-tailed unpaired Student's t-tests were used. For multiple group comparisons, one-way
643 ANOVA followed by Dunnet's or Sidak's post hoc tests were applied as appropriate. Results were
644 polled from a minimum of n=3 independent experiments and presented as mean ± standard error
645 of the mean (SEM). P-values < 0.05 were considered statistically significant. The number of
646 replicates (n) and details of the specific tests applied are provided in figure legends.
647
648

Funding Declaration

Support for this work was provided by National Institutes of Health (NIH) grants F32AG072826 (MRB) and R01AG068063 (TJC). This study was supported by the National Institute on Aging of the National Institutes of Health under Award Number P30AG072958 (NIAP30AG072958) (MRB, MA, and JHT), Alzheimer's Association grants AARG-22-924321 (TJC) AARF22926617 (JHT), and CurePSP grant 656-2018-06 (TJC). The content is solely the responsibility of the authors and does not necessarily represent the official views of the National Institutes of Health.

Acknowledgements

The Andor Dragonfly microscope was funded with support from National Institutes of Health grant S10OD030223. The Zeiss LSM 980 microscope was funded with support from NIH grant S10 OD032388. We would also like to thank Kinsley Adams for her expertise and assistance with the hippocampal organotypic slice cultures. We would also like to thank the University of Pennsylvania (Center for Neurodegenerative Disease Research brain bank) for providing human control and AD cortex lysates. Lastly, we would like to thank the University of North Carolina Translational Pathology Laboratory for providing AD hippocampal brain sections.

Conflict of interest

The authors declare that they have no conflicts of interest with the contents of this article.

Author Contributions

MRB designed and performed most experiments. MA, JS, and BB designed and carried out ex vivo organotypic slices experiments and imaging. KP performed all immunohistochemistry and

672 confocal imaging of human post-mortem brain. CO assisted with co-immunoprecipitation
673 experiments and post-synaptic density preparations. CO and JHT performed human brain
674 fractionation and immunoblots. EP performed all protein purification and carried out the
675 Thioflavin T aggregation assays. JMM assisted with multi-electrode array recordings and
676 analyses. XT prepared all plasmid and lentiviral constructs for all experiments. DK and HT
677 designed and performed the QBI293 experiments comparing various P301 and S320 tau mutants.
678 JHT, JS, NB, and BB provided additional experimental guidance and interpretation. MRB and TJC
679 prepared the manuscript and figures. TJC directed and supervised the study. All authors consented
680 and contributed to the final version of the manuscript.
681
682

683 **Figures and Figure Legends**

Bryan et al., Figure 1.

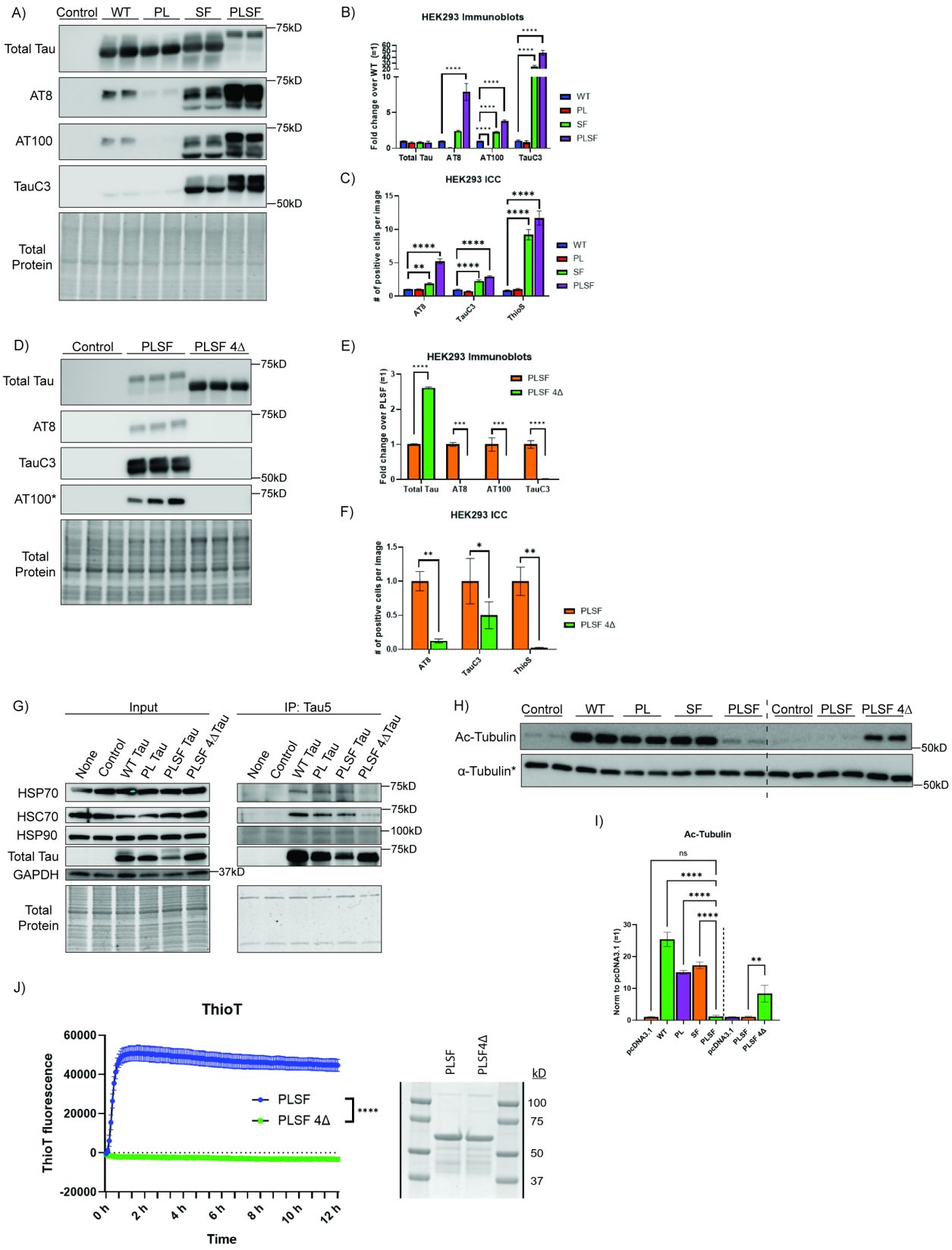

685 **Figure 1: Abrogating tau binding to heat shock proteins alleviates pathology in a PL-SF tau**
686 **aggregation model.**
687 **A)** Representative immunoblots (RIPA fraction) of QBI-293 cells transfected with 2N4R WT,
688 P301L, S320F, or P301L-S320F tau. **B)** Immunoblot quantification of total tau, p-tau (AT8 and
689 AT100), and cleaved tau (TauC3) in RIPA fraction. N=4 per condition; **C)** Immunocytochemistry
690 quantification of QBI-293 cells transduced with WT, P301L, S320F, or PL-SF tau labeled with
691 AT8, TauC3, or ThioS. N=48 FOVs per condition. *= p-value significant by one-way ANOVA.
692 Representative images found in Supplemental Figure 1. **D)** Representative immunoblots (RIPA
693 fraction) of QBI-293 cells transfected with 2N4R P301L-S320F tau or P301L-S320F 4Δ (deletion
694 of I277/278, I308/V309 residues). *AT100 was run on a separate blot with the exact same lysates
695 to improve detection. **E)** Immunoblot quantification of total tau, p-tau (AT8 and AT100), and
696 cleaved tau (TauC3) in RIPA soluble fractions. N=3 per condition. **F)** Immunocytochemistry
697 quantification of QBI-293 cells transduced with 2N4R PL-SF or PL-SF 4Δ tau labeled with AT8,
698 TauC3, or ThioS. N=16 FOVs per condition. *= p-value significant by unpaired Student's t-test.
699 Representative images found in Supplemental Figure 3. **G)** Co-immunoprecipitation of QBI-293
700 cells transfected with WT, P301L, PL-SF, or PL-SF 4Δ tau. Tau5 antibody was used to IP tau and
701 immunoblots were probed with total tau (rabbit polyclonal) and Hsp70, Hsc70, and Hsp90
702 antibodies. **H)** Representative immunoblots of QBI-293 cells transfected with 2N4R tau variants
703 and probed with acetyl-tubulin and total alpha-tubulin antibodies. Note: Acetyl tubulin and alpha
704 tubulin blots were run separately with the same lysates to improve detection. **I)** Quantification of
705 acetyl-tubulin across all 2N4R tau variants. -- line signifies separate sets of transfections in panel
706 I and J. N=4 per condition; *= p-value significant by one-way ANOVA. Control= empty plasmid
707 vector (pcDNA3.1)**.** **J)** Quantification of in vitro Thioflavin T aggregation assay using purified

708 protein from PLSF and PLSF 4Δ. N=4 replicates per condition. *= significant by unpaired student

709 t-test at 12hr timepoint. Coomassie (right) shows equal protein loading into reactions.

710

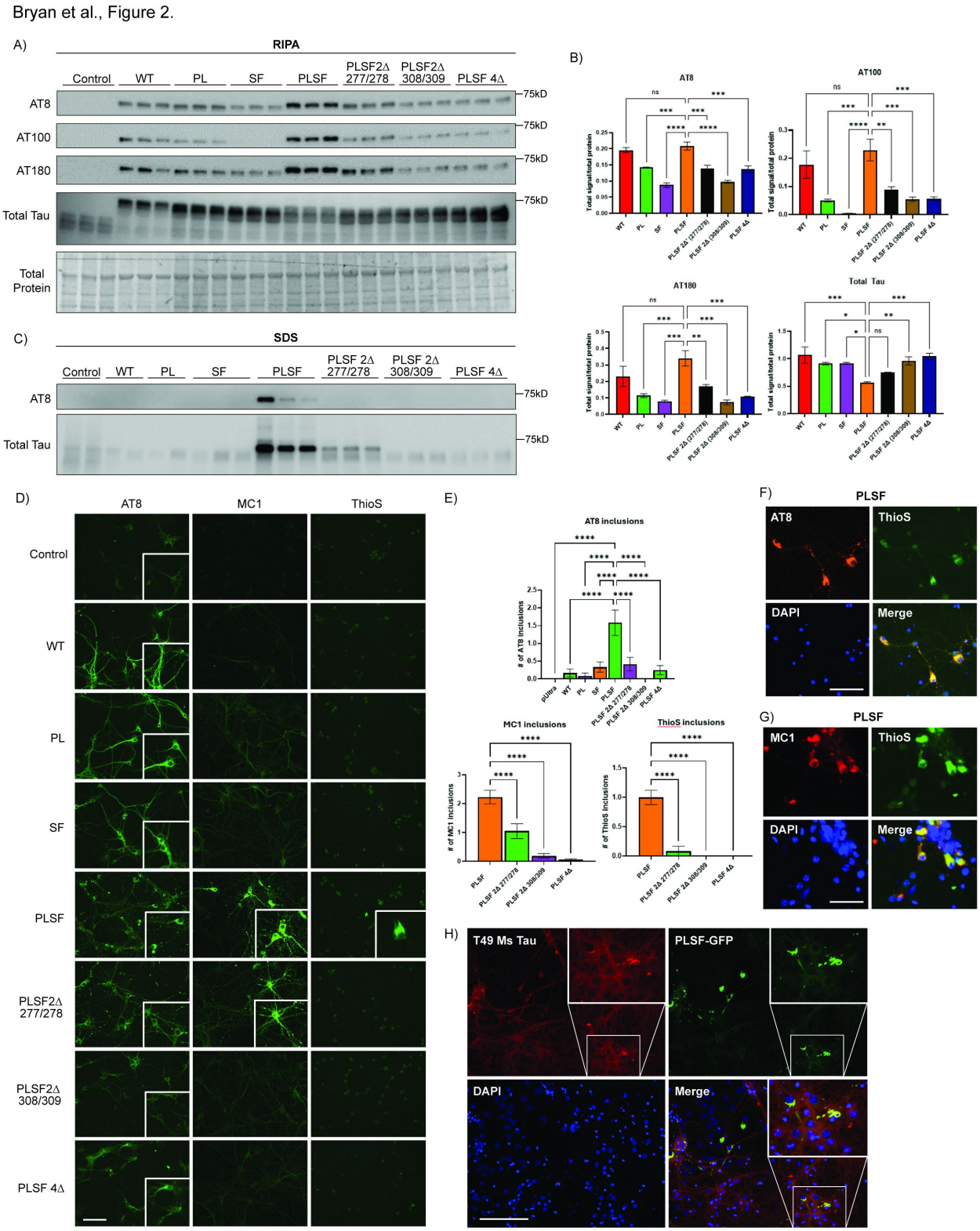

Figure 2: Development and characterization of a PL-SF tau aggregation model in primary cortical neurons.

714 **A)** Representative RIPA-soluble immunoblots of DIV10 primary cortical neurons transduced with
715 lentiviruses expressing 2N4R WT, P301L, S320F, P301L-S320F, or PL-SF 2Δs (R2 and R3) and
716 4Δ tau variants. **B)** Quantification of AT8, AT100, AT180, and total tau immunoblots in primary
717 cortical neurons (RIPA fraction). N=3 per condition; *= p-value significant by one-way ANOVA.
718 **C)** Representative SDS-soluble immunoblots of DIV10 primary cortical neurons transduced with
719 lentiviruses expressing 2N4R WT, P301L, S320F, P301L-S320F, or PL-SF 2Δ and 4Δ tau variants.
720 N=2 for control, WT, and P301L; N=3 for other variants. **D)** Representative immunocytochemistry
721 images of 2N4R tau variants labeled with AT8 (p-tau), MC1 (conformational tau), ThioS
722 (aggregated tau) in GFP. Scale bar= 125 µm. **E)** Quantification of the number of AT8, MC1, and
723 ThioS inclusions in PL-SF and PL-SF 2Δ (R2 and R3) and 4Δ variants. N=12-24 FOVs per
724 condition. *= significant by one-way ANOVA. **F, G)** Representative immunocytochemistry
725 images of PL-SF tau displaying colocalization between F) AT8 (p-tau) or G) MC1 (conformational
726 tau) with ThioS (aggregated tau). Scale bar= 50um. **H)** Representative immunocytochemistry of
727 PL-SF GFP colocalized with T49 tau (mouse-specific). Scale bar= 125 µm. Control= empty viral
728 vector (pUltra)**.**

Bryan et al., Figure 3.

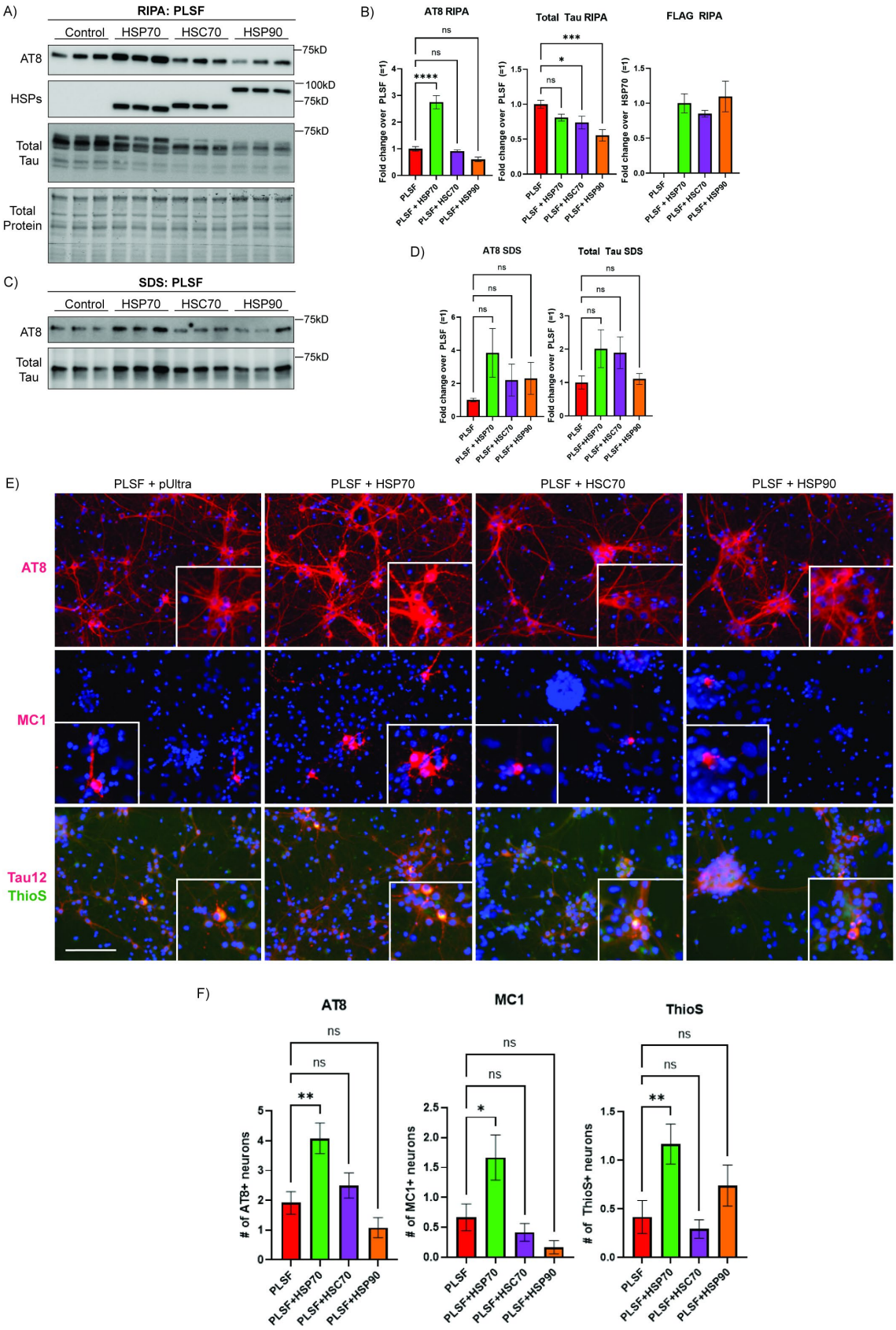

730 **Figure 3: Hsp70 exacerbates tau hyperphosphorylation and aggregation.**

731 **A)** Representative immunoblots of 2N4R PL-SF tau co-transduced with HSP70, HSC70, and
732 HSP90 in DIV10 primary cortical neurons (RIPA fraction). **B)** Quantification of AT8 (p-tau), total
733 tau (rabbit polyclonal), or Hsp70, Hsc70, Hsp90 (FLAG-tagged) in the RIPA fraction. N=6 per
734 condition. *= p-value significant by one-way ANOVA. **C)** Representative immunoblots of 2N4R
735 PL-SF tau co-transduced with HSP70, HSC70, and HSP90 in DIV10 primary cortical neurons
736 (SDS fraction). **D)** Quantification of AT8 (p-tau), total tau (rabbit polyclonal) in the SDS fraction.
737 N=6 per condition. ns= p-value is not significant by one-way ANOVA. **E)** Representative
738 immunocytochemistry images of primary cortical neurons co-transduced 2N4R PL-SF tau and
739 HSP70, HSC70, or HSP90 labeled with AT8, MC1, Tau12 (RFP) or ThioS (GFP). Scale bar= 125
740 μm. **F)** Quantification of MC1, AT8, and ThioS positive inclusions in primary cortical neurons
741 co-transduced 2N4R PL-SF tau and either HSP70, HSC70, or HSP90. n=12 FOVs per condition.
742 *= p-value significant by one-way ANOVA. Control= empty viral vector (pUltra)**.**

743

Bryan et al., Figure 4.

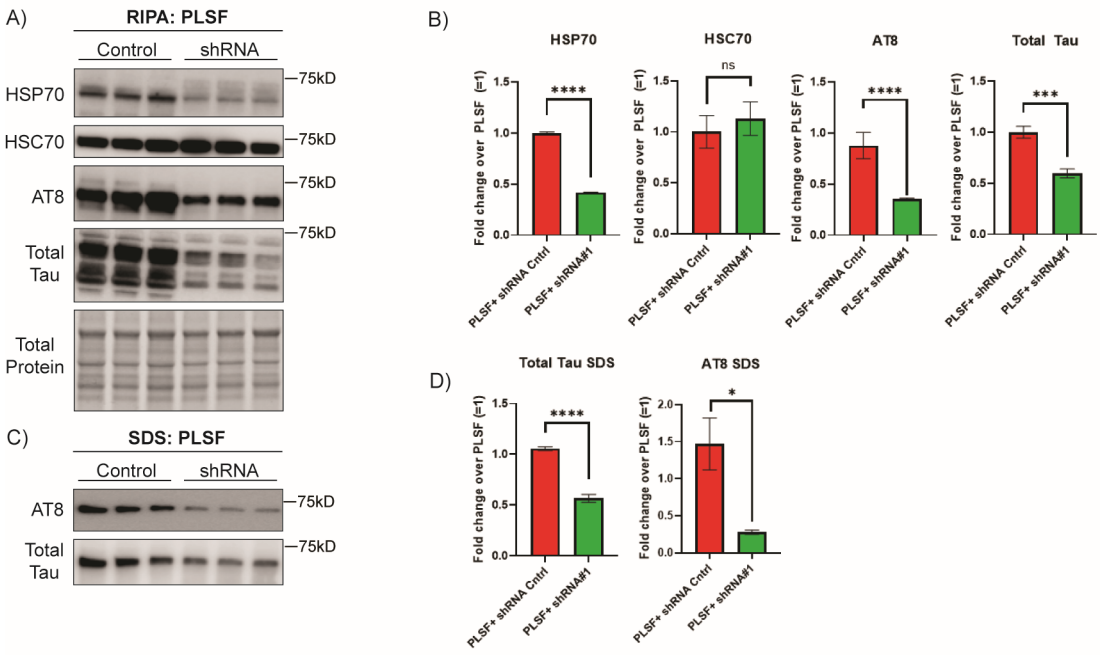

Figure 4: Reducing Hsp70 can suppress tau hyper-phosphorylation and aggregation. **A)** Representative immunoblots of 2N4R PL-SF tau co-transduced with a shRNA against HSP70 in DIV10 primary cortical neurons (RIPA fraction). **B)** Quantification of AT8 (p-tau), total tau (rabbit polyclonal) and endogenous Hsp70 and Hsc70 in the RIPA fraction. N=3. **C)** Representative immunoblots of 2N4R PL-SF tau co-transduced a shRNA against HSP70 in DIV10 primary cortical neurons (SDS fraction). **D)** Quantification of AT8 (p-tau), total tau (rabbit polyclonal) in the SDS fraction. N=3. *= p-value significant by unpaired Student's t-test. Control= empty viral vector (pUltra)**.**

Bryan et al., Figure 5.

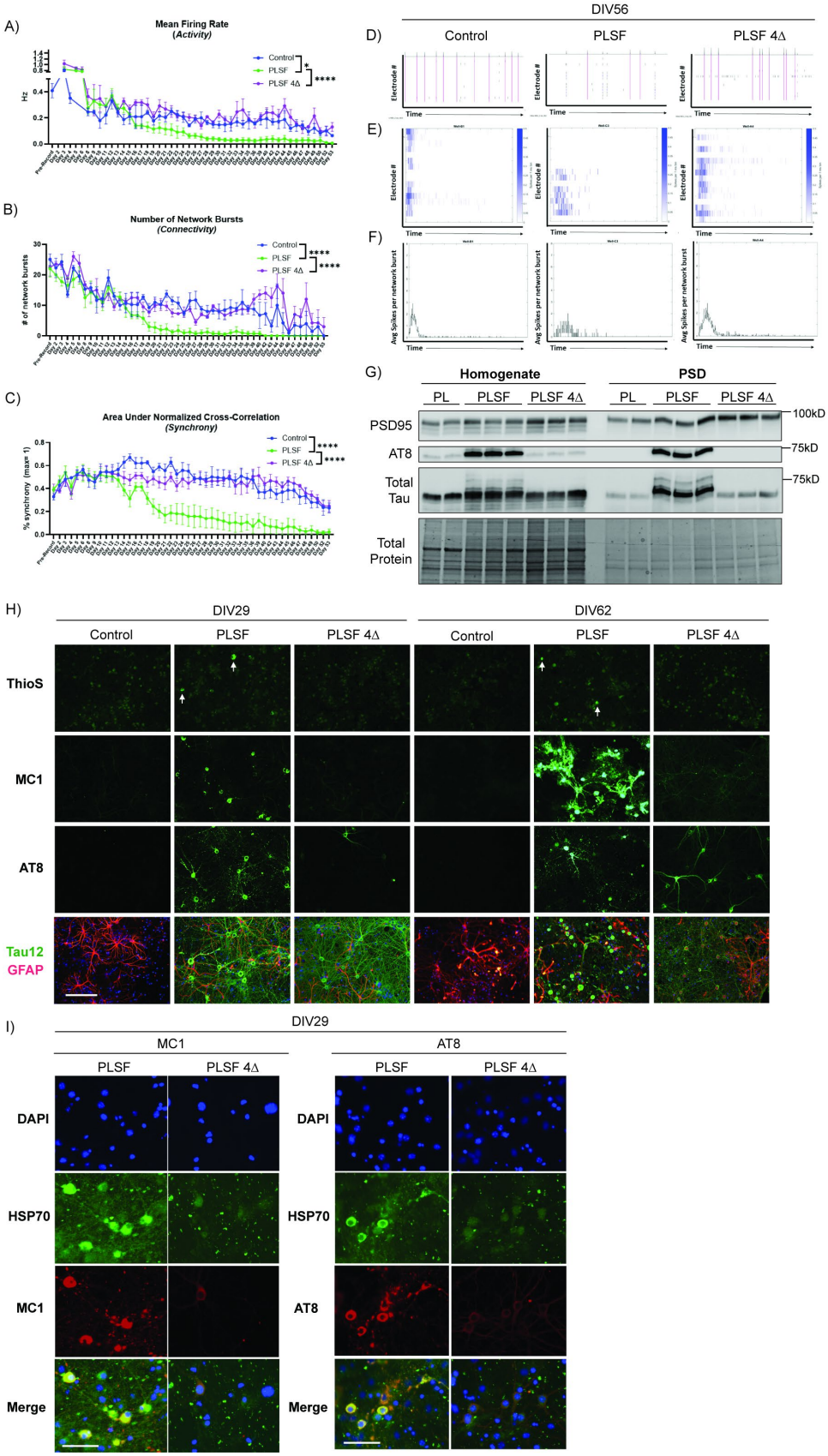

754 **Figure 5: Mature tau aggregates cause functional deficits in neurons that are reversed by**
755 **abrogating tau-Hsp binding.**
756 **A-C)** Quantification of neuronal activity comparing PL-SF to PL-SF 4Δ across 53 days of multi-
757 electrode array recording starting at DIV18 following initial pre-recording. A) Mean firing rate-
758 activity B) Number of network bursts- connectivity C) Area under normalized cross-correlation-
759 synchrony. N=4 replicate wells per condition. *= p-value significant by one-way ANOVA. **D-F)**
760 Representative raster and network burst plots at DIV54 (day 36 of recording) comparing empty
761 control (pUltra) to PL-SF and PL-SF 4Δ. D) Number of network bursts across electrodes over time
762 (pink lines) E) number of spikes across electrodes over time F) Average number of spikes per
763 network burst over time. **G)** Representative immunoblot of isolated post synaptic density (PSD)
764 in DIV18 primary cortical neurons transduced with lentiviruses expressing P301L, PL-SF, or PL-
765 SF 4Δ. Immunoblot was probed with PSD95, AT8 (p-tau), and rabbit polyclonal tau (total tau). **H)**
766 Representative 20X immunocytochemistry images of primary cortical neurons comparing empty
767 vector control (pUltra) to PL-SF and PL-SF 4Δ tau variants at DIV29 and DIV62. Neurons were
768 labeled with ThioS (aggregated tau), MC1 (conformational tau), AT8 (p-tau), and Tau12 (total
769 tau) in GFP. Tau12 was co-labeled with GFAP (RFP) to label astrocytes. Scale bar= 125 µm. **I)**
770 Representative immunocytochemistry images of primary cortical neurons comparing PL-SF and
771 PL-SF 4Δ at DIV29. Neurons were labeled with endogenous Hsp70 (GFP), MC1 or AT8 (RFP),
772 and DAPI (BFP). Scale bar= 50 µm. Control= empty viral vector (pUltra)**.**

Bryan et al., Figure 6.

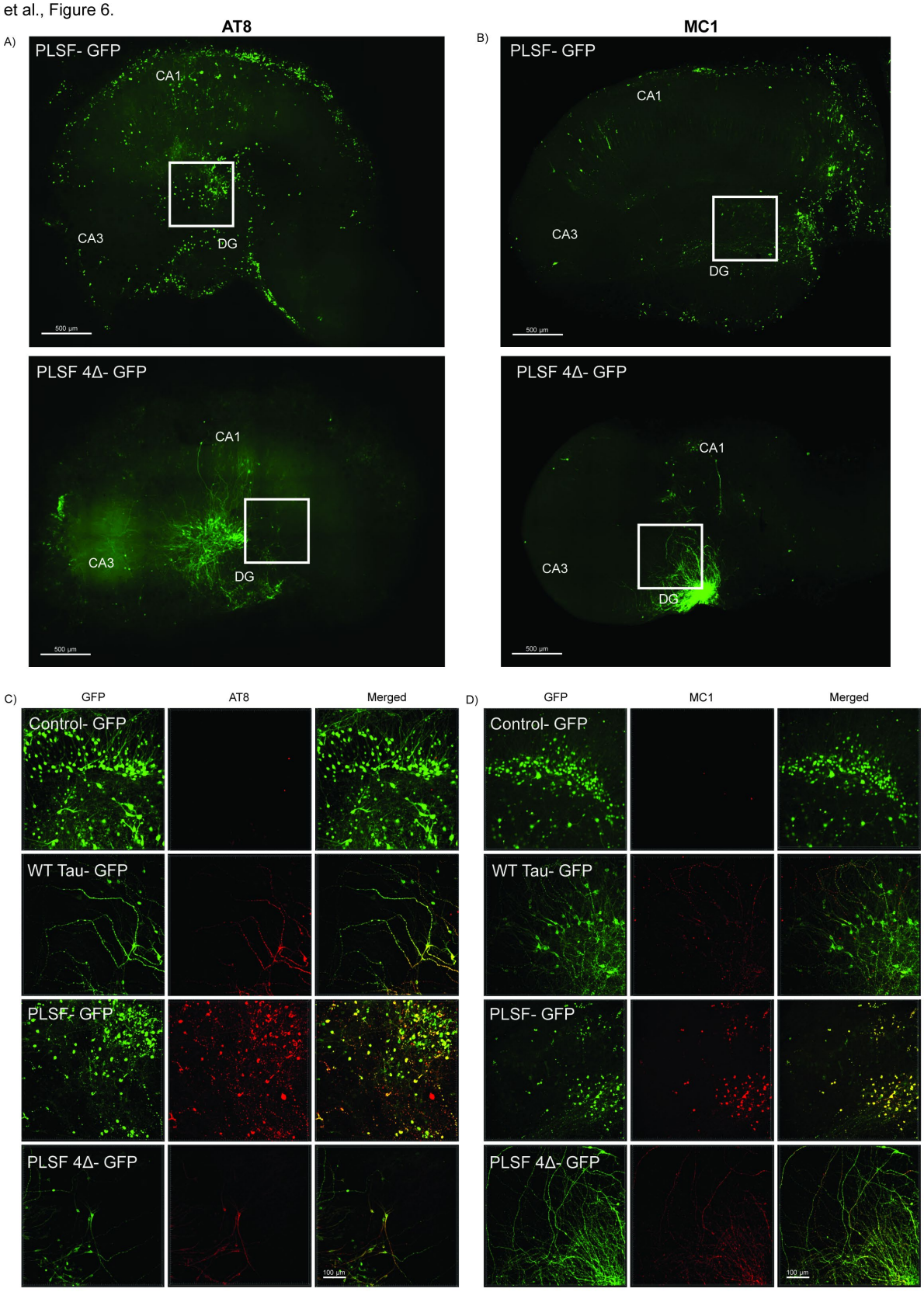

774 **Figure 6: Abrogating tau-Hsp binding suppresses tau pathology in three-dimensional**
775 **organotypic hippocampal slice cultures.**
776 Rat hippocampal slices were processed for immunocytochemistry after 9 weeks in culture
777 following lentiviral infection of eGFP empty vector control, wild-type tau, PL-SF tau, and PL-SF
778 4Δ. **A, B)** Immunocytochemistry of the entire hippocampal slice following labeling of reveal
779 sufficient expression of PL-SF and PL-SF 4Δ lentiviruses (GFP). Left- AT8 staining; Right- MC1
780 staining. CA1, CA3, and DG regions are labeled in white font. White boxes denote magnified
781 images in panel C, D. Scale bar= 500 µm. **C, D)** Representative immunocytochemistry images of
782 C) AT8 and D) MC1 labeled in RFP for empty vector control, wild-type tau, PL-SF tau, and PL-
783 SF 4Δ taken from the dentate gyrus (DG) region of the hippocampal slice culture (inset white
784 boxes from A, B). Scale bar= 100 µm.

Bryan et al., Figure 7

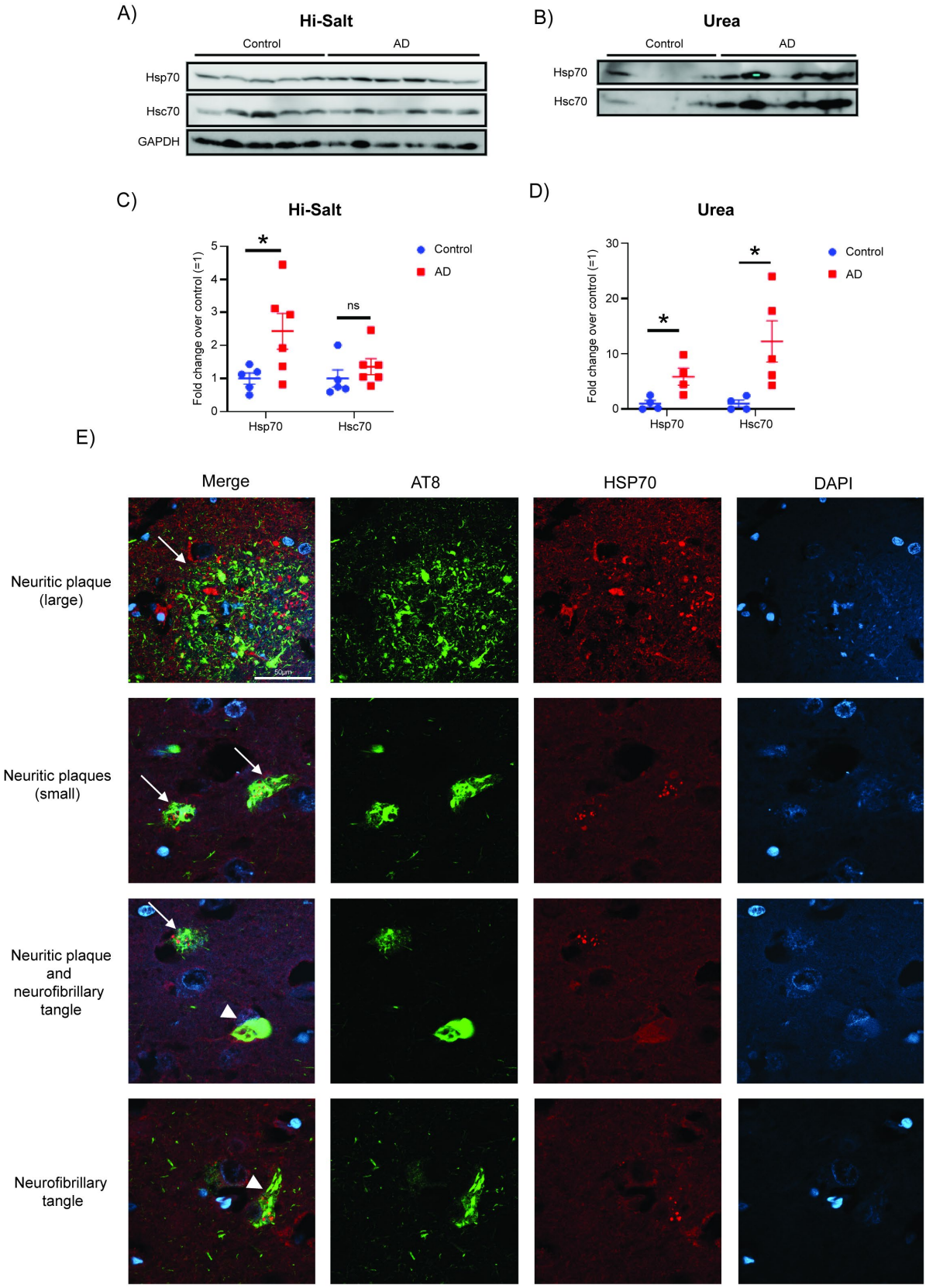

786 **Figure 7: HSP70 is upregulated in human AD brain and intercalates within tau aggregates.**
787 **A)** Hi-Salt soluble immunoblots from control (n=5) and AD (n=6) cortical lysates probed for
788 Hsp70, Hsc70, and GAPDH. **B)** Quantification of hi-salt immunoblots. *= p-value significant by
789 unpaired Student's t-test. **C)** Urea soluble immunoblots from control (n=4) and AD (n=5) probed
790 for Hsp70 and Hsc70. **D)** Quantification of urea immunoblots. *= p-value significant by unpaired
791 Student's t-test. Overexposed Hsp70 AD sample in urea was excluded from quantification. **E)**
792 Representative 63X confocal single-plane z-stacks from AD human hippocampus stained with
793 AT8 (p-tau) and Hsp70. White arrow label neuritic plaques and white arrowheads label NFTs.
794
795
796
797

Bryan et al., Supplemental Figure 1.

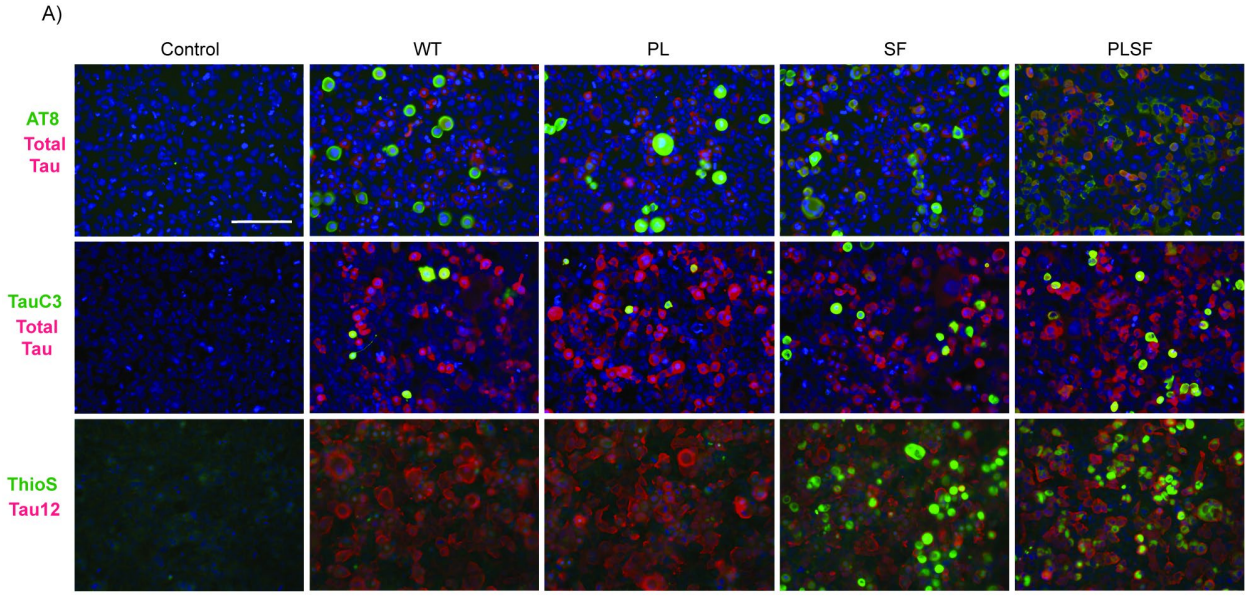

Supplemental Figure 1: Accelerated PL-SF aggregation compared to single tau mutants in immortalized cell lines.

A) Representative immunocytochemistry images from QBI-293 cells expressing empty vector (pcDNA) or WT, PL, SF, and PL-SF tau variants. Cells were labeled with AT8 (p-tau) or TauC3 (C-terminal cleaved tau) with rabbit polyclonal tau (total tau) and ThioS with Tau12 (human tau). Quantification of images is found in Figure 1C. Control= empty plasmid vector (pcDNA3.1). Scale bar= 125 µm.

Bryan et al., Supplemental Figure 2.

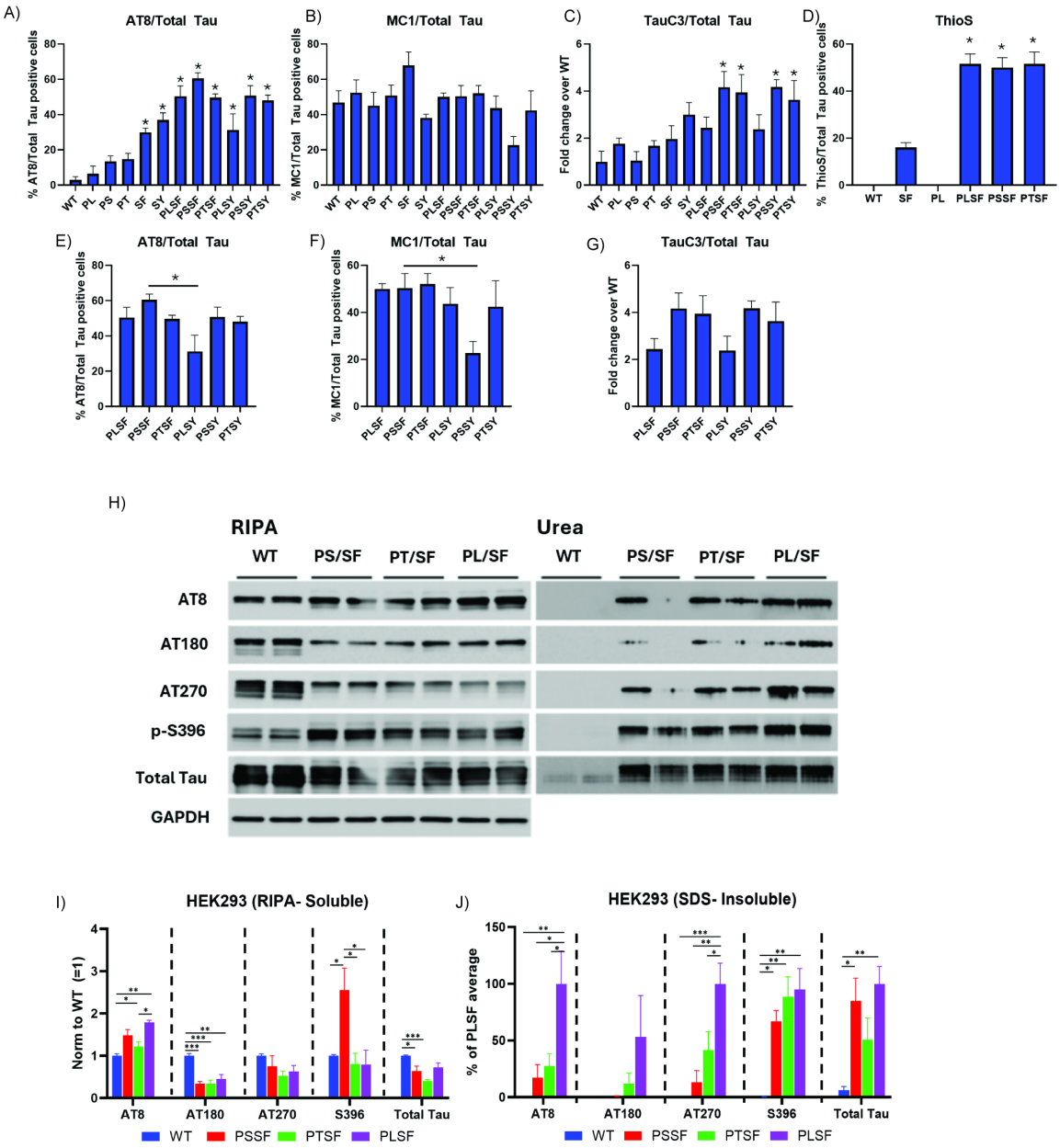

Supplemental Figure 2: Immunoblotting analysis of a panel of P301 and S320 single and combination mutants.

A-G) Quantification of AT8, MC1, TauC3, and ThioS immunocytochemistry in QBI-293 cells expressing various P301 and S320 mutants alone or in combination. Panels E-G are subsets of data from A-C to perform additional comparisons among combinatorial mutants. Representative

815 images not shown. Error bars= SEM. *= significant difference by one-way ANOVA. **H)**
816 Representative immunoblots from QBI-293 cells expressing wild-type, P301S/S320F,
817 P301T/S320F, and P301L/S320F tau variants. RIPA (soluble) and urea (insoluble) fractions were
818 analyzed by immunoblotting for p-tau epitopes (AT8, AT180, AT270, p-396) and total tau (rabbit
819 polyclonal). **I, J)** Quantification of RIPA soluble and urea (insoluble) fractions. Error bars= SEM.
820 *= significant difference by one-way ANOVA.
821
822
823
824
825
826

Bryan et al., Supplemental Figure 3.

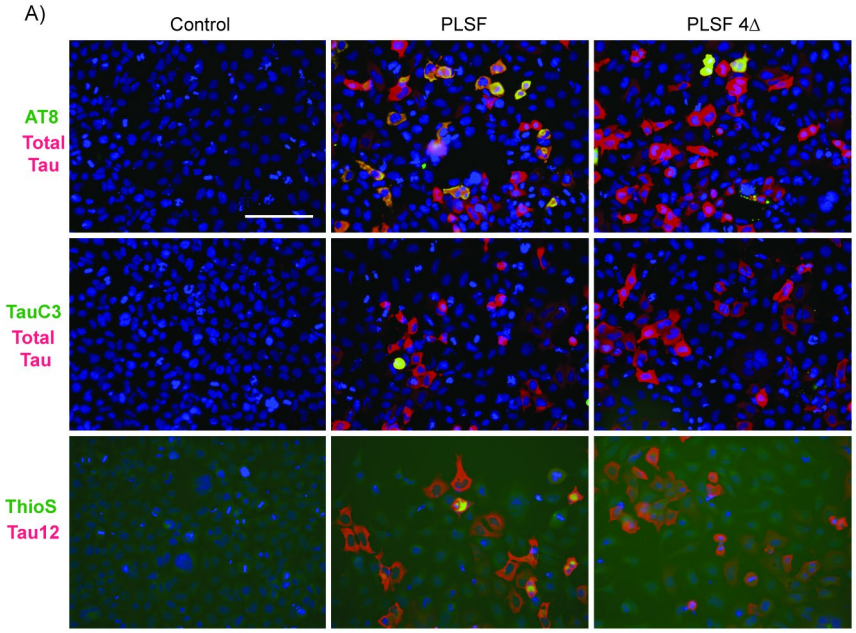

827

828 **Supplemental Figure 3: Abrogating Hsp binding via the PL-SF 4Δ variant suppresses the**

829 **accumulation of pathological tau.**

830 Representative immunocytochemistry images from QBI-293 cells expressing tau PL-SF and PL-

831 SF 4Δ tau variants. Cells were probed with AT8 (p-tau), TauC3 (C-terminal cleaved tau) with

832 rabbit polyclonal tau (total tau), and ThioS with Tau12 (human tau). Quantification of images is

833 found in Figure 1F. Control= empty plasmid vector (pcDNA3.1)**.** Scale bar= 125 µm.

Bryan et al., Supplemental Figure 4.

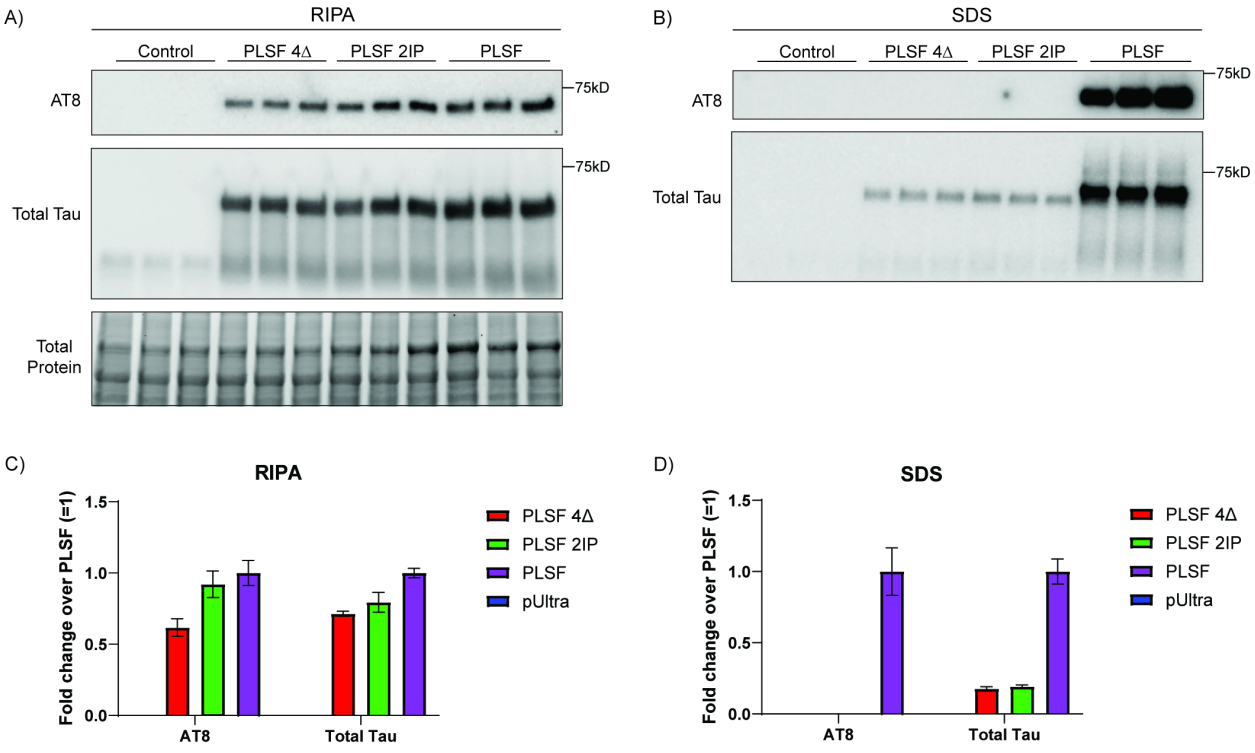

Supplemental Figure 4: PLSF containing the β-structure breaking mutations, I277P/I308P, prevents tau aggregation similar to PLSF 4Δ.

A) Representative RIPA immunoblot of primary neurons transduced with empty control, PLSF 4Δ-eGFP, PLSF I277P/I308P (2IP), or PLSF-eGFP and probed for p-tau (AT8) and total tau (rabbit polyclonal). **B)** Quantification of AT8 and total tau in RIPA fraction. **C)** Representative SDS immunoblot of primary neurons transduced with empty control, PLSF 4Δ-eGFP, PLSF I277P/I308P (2IP), or PLSF-eGFP and probed for p-tau (AT8) and total tau (rabbit polyclonal. **D)** Quantification of SDS fraction. *= significant difference by one-way ANOVA.

Bryan et al., Supplemental Figure 5.

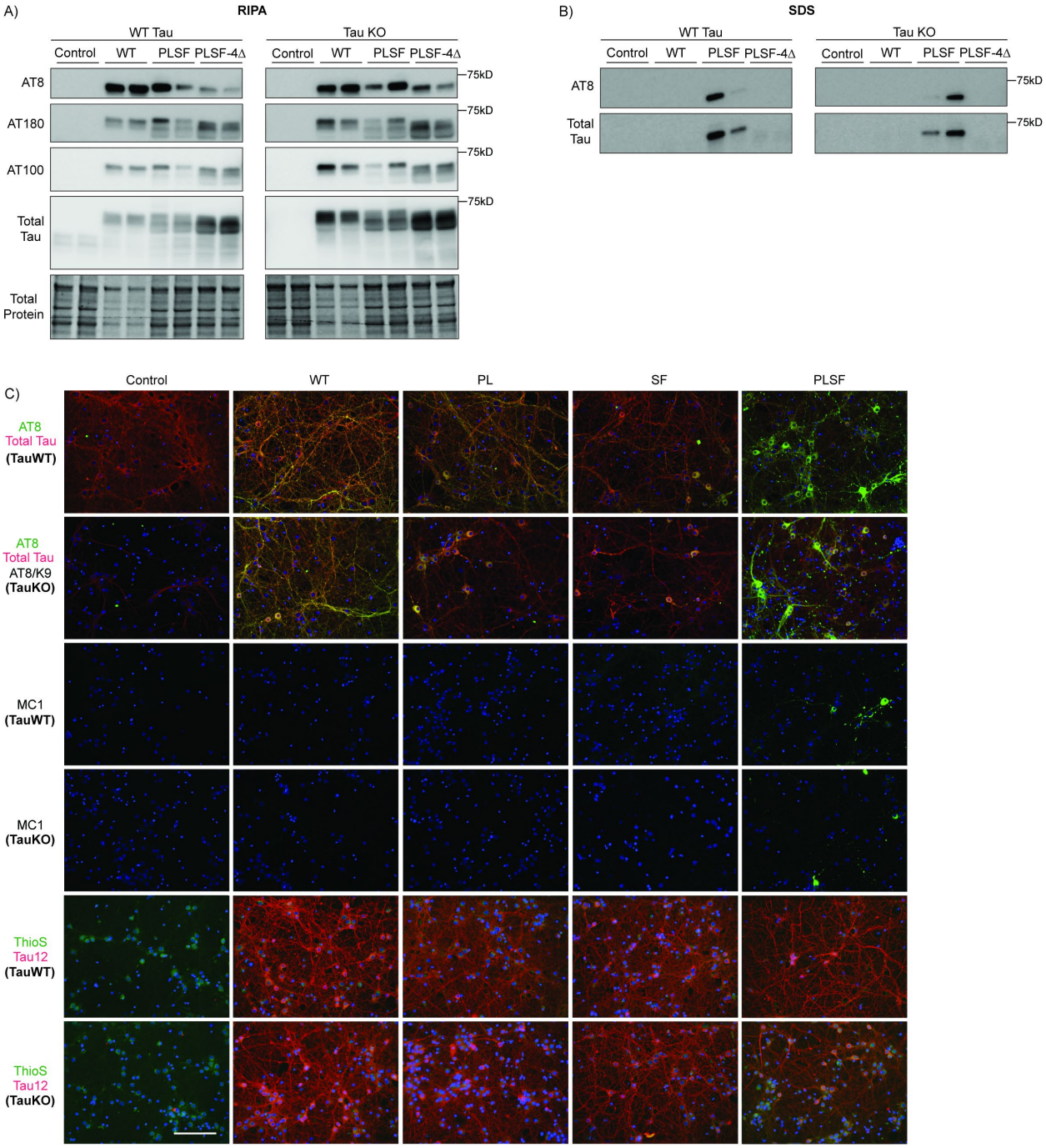

843

844 **Supplemental Figure 5: PL-SF aggregates emerge similarly in either wild-type or tau**

845 **knockout neurons lacking endogenous mouse tau.**

846 **A)** RIPA (soluble) immunoblot of wild-type tau and tau knockout neurons probed with p-tau

847 (AT8, AT180, AT100) and total tau (rabbit polyclonal). **B)** SDS (insoluble) immunoblot of wild-

848 type tau and tau knockout neurons probed with p-tau (AT8) and total tau (rabbit polyclonal). **C)**
849 Representative immunoblotting images of wild-type, P301L, S320F, and P301L/S320F tau
850 variants in wild-tau-expressing or tau knockout neurons. Neurons were labeled with AT8 (GFP)
851 and rabbit polyclonal total tau (RFP), MC1 (GFP), or ThioS (GFP) and Tau12 (RFP). Scale bar=
852 125 µm. Control= empty viral vector (pUltra)**.**
853
854
855
856
857
858
859
860
861
862
863

Bryan et al., Supplemental Figure 6.

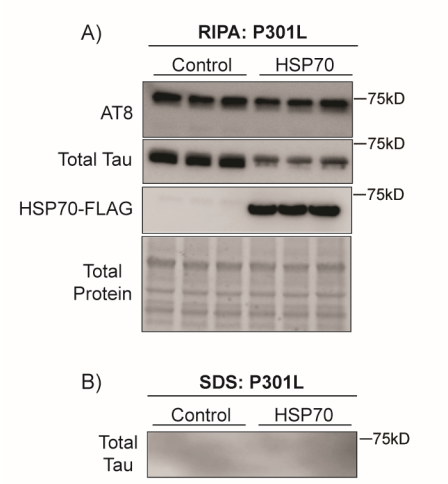

Supplemental Figure 6: Overexpression of HSP70 in P301L-expressing neurons does not promote tau phosphorylation or aggregation.

A) RIPA (soluble) immunoblot of primary neurons following 1-week of lentiviral co-transduction with P301L tau and HSP70. Blot was probed with p-tau (AT8), total tau (rabbit polyclonal), and M2 FLAG (Hsp70-FLAG). **B)** SDS (insoluble) immunoblot of primary neurons was unable to detect insoluble tau species with total tau antibody (rabbit polyclonal). Control= empty viral vector (pUltra)**.**

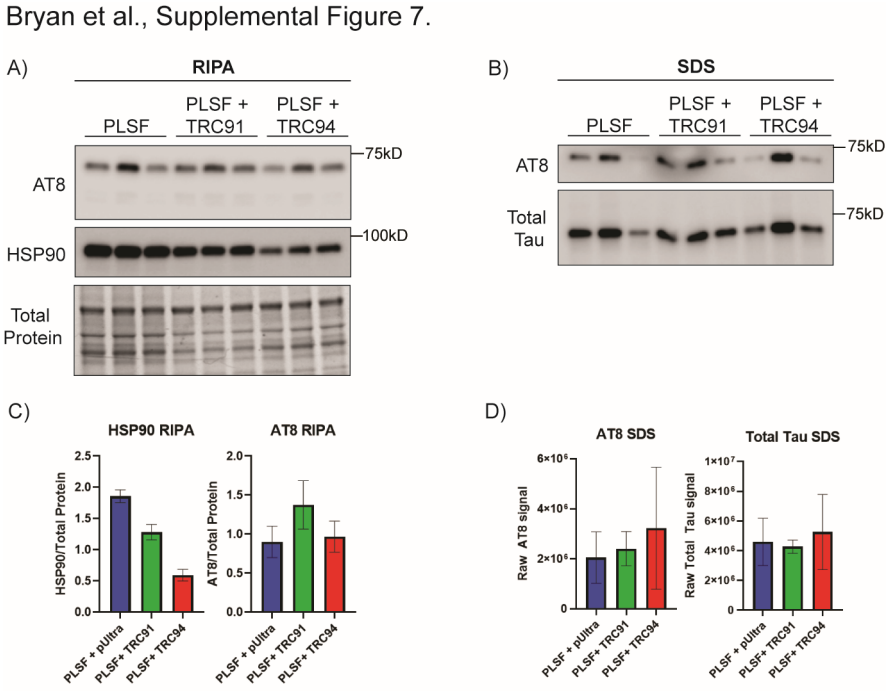

Supplemental Figure 7: HSP90 depletion does not alter phosphorylated or aggregated PL-SF tau.

A) RIPA (soluble) immunoblot of primary neurons probed with p-tau (AT8) and Hsp90 following 1-week of lentiviral HSP90 knockdown with two shRNAs (called TRC91 and TRC94). **B)** SDS (insoluble) immunoblot of primary neurons probed with p-tau (AT8) and total tau (rabbit polyclonal) following 1-week of lentiviral HSP90 knockdown. **C)** Quantification of AT8 and Hsp90 in the RIPA fraction. Error bars= SEM. **D)** Quantification of AT8 and total tau (rabbit polyclonal) in SDS fraction. *Note: Only TRC94, and not TRC91, HSP90 shRNA was able to reduce Hsp90 expression.

Bryan et al., Supplemental Figure 8.

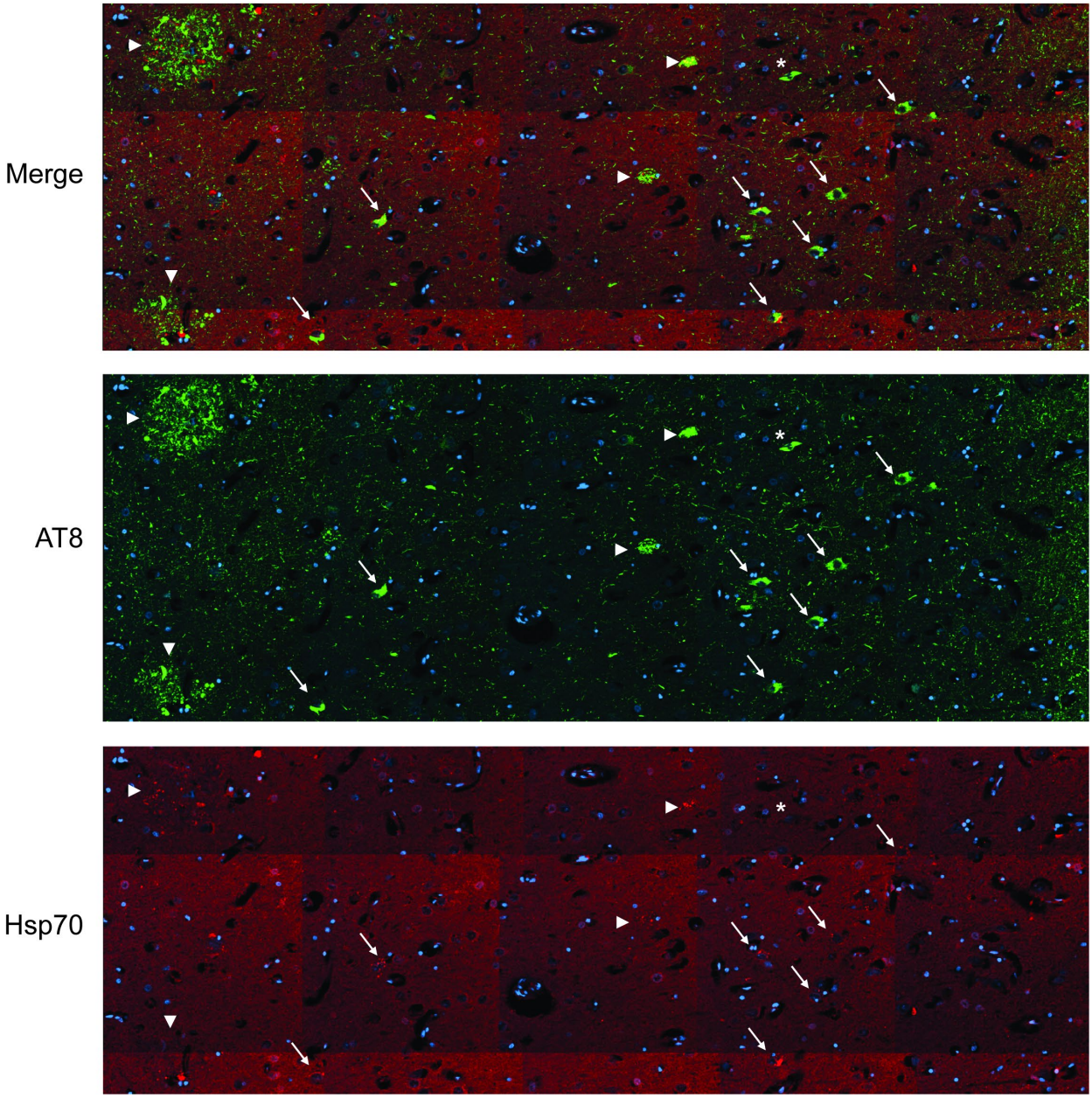

Supplemental Figure 8: Hsp70 foci accumulation within neuritic plaques and neurofibrillary tangles in human AD brain

A) Representative stitched widefield images of a human AD patient hippocampus labeled with AT8 (GFP) and Hsp70 (RFP). AT8/Hsp70 positive plaques are labeled with white arrowheads. AT8/Hsp70 positive tangles are labeled with white arrows. * = a single AT8 positive tangle that is

absent for Hsp70 foci.

Table 1: Primers used for vector construction

Primer	Sequence
d277-278F	AATAAGAAGCTGGATCTTAGCAACGTC
d277-278R	CTGCACCTTCCCGCCTCC
d308-309F	TACAAACCAGTTGACCTGAGCAAG
d308-309R	TTGCACACTGCCGCCTCC
Tau F	CCGACCGGTGCCACCATGGCTGAGCCCCGCCAG
Tau R	CGCGTCGACTCACAAACCCTGCTTGGCCAGG
I308P-F	CAGTGTGCAAccgGTCTACAAACCAGTTGACCTGAGcaagg
I308P-R	CCGCCTCCCAGGACGtgtttg
I277P-F	GAAGGTGCAGccgATTAATAAGAAGCTGGATCTTAGCAACGtccagtcc
HSP70-F	GCGACCGGTGCCACCATGGATTACAAGGATGACGACGATAAGATGGCCAAAGCCGCGGCGATCG
HSP70-R	TCGGTCGACCTAATCTACCTCCTCAATGGTGGGGCC
HSC70-F	GCGACCGGTGCCACCATGGATTACAAGGATGACGACGATAAGATGTCCAAGGGACCTGCAGTTGG
HSC70-R	TCGGTCGACATCAACCTCTTCAATGGTGGGCCC
Hsp90-F	GCGACCGGTGCCACCATGGATTACAAGGATGACGACGATAAG
Hsp90-R	GCGGTCGACGCTAGTCTACTTCTTCCATGCGTGATGTG

References

1. Strang, K. H., Golde, T. E. & Giasson, B. I. MAPT mutations, tauopathy, and mechanisms of neurodegeneration. *Lab. Investig.* **99**, 912–928 (2019).

2. Trzeciakiewicz, H. *et al.* An HDAC6-dependent surveillance mechanism suppresses tau-mediated neurodegeneration and cognitive decline. *Nat Commun* **11**, 5522 (2020).

3. Koller, E. J. *et al.* Combining P301L and S320F tau variants produces a novel accelerated model of tauopathy. *Hum Mol Genet* **28**, 3255–3269 (2019).

4. Strang, K. H. *et al.* Distinct differences in prion-like seeding and aggregation between tau protein variants provide mechanistic insights into tauopathies. *J Biological Chem* **293**, 2408–2421 (2017).

5. Croft, C. L. *et al.* rAAV-based brain slice culture models of Alzheimer's and Parkinson's disease inclusion pathologies. *J Exp Medicine* **216**, 539–555 (2019).

6. Xia, Y. *et al.* Pathogenic tau recruits wild-type tau into brain inclusions and induces gut degeneration in transgenic SPAM mice. *Commun Biology* **5**, 446 (2022).

7. Beckman, D. *et al.* Temporal progression of tau pathology and neuroinflammation in a rhesus monkey model of Alzheimer's disease. *Alzheimer's Dement.* **20**, 5198–5219 (2024).

8. Kaniyappan, S. *et al.* FRET-based Tau seeding assay does not represent prion-like templated assembly of Tau fibers. *Biorxiv* 2020.03.25.998831 (2020) doi:10.1101/2020.03.25.998831.

9. Xu, P. *et al.* Allosteric inhibition of HSP70 in collaboration with STUB1 augments enzalutamide efficacy in antiandrogen resistant prostate tumor and patient-derived models. *Pharmacol. Res.* **189**, 106692 (2023).

10. Li, X. *et al.* Analogues of the Allosteric Heat Shock Protein 70 (Hsp70) Inhibitor, MKT-077, As Anti-Cancer Agents. *Acs Med Chem Lett* **4**, 1042–1047 (2013).

11. Miyata, Y. *et al.* Synthesis and Initial Evaluation of YM-08, a Blood-Brain Barrier Permeable Derivative of the Heat Shock Protein 70 (Hsp70) Inhibitor MKT-077, Which Reduces Tau Levels. *Acs Chem Neurosci* **4**, 930–939 (2013).

12. Moradi-Marjaneh, R., Paseban, M. & Marjaneh, M. M. Hsp70 inhibitors: Implications for the treatment of colorectal cancer. *IUBMB Life* **71**, 1834–1845 (2019).

13. Abisambra, J. *et al.* Allosteric Heat Shock Protein 70 Inhibitors Rapidly Rescue Synaptic Plasticity Deficits by Reducing Aberrant Tau. *Biol Psychiat* **74**, 367–374 (2013).

950 14. Biamonte, M. A. *et al.* Heat Shock Protein 90: Inhibitors in Clinical Trials. *J. Med. Chem.*
951 **53**, 3–17 (2010).

952 15. Jinwal, U. K. *et al.* Hsc70 Rapidly Engages Tau after Microtubule Destabilization*. *J Biol*
953 *Chem* **285**, 16798–16805 (2010).

954 16. Kundel, F. *et al.* Hsp70 Inhibits the Nucleation and Elongation of Tau and Sequesters Tau
955 Aggregates with High Affinity. *ACS Chem. Biol.* **13**, 636–646 (2018).

956 17. Patterson, K. R. *et al.* Heat Shock Protein 70 Prevents both Tau Aggregation and the
957 Inhibitory Effects of Preexisting Tau Aggregates on Fast Axonal Transport. *Biochemistry* **50**,
958 10300–10310 (2011).

959 18. Petrucelli, L. *et al.* CHIP and Hsp70 regulate tau ubiquitination, degradation and aggregation.
960 *Hum Mol Genet* **13**, 703–714 (2004).

961 19. Fontaine, S. N. *et al.* DnaJ/Hsc70 chaperone complexes control the extracellular release of
962 neurodegenerative-associated proteins. *EMBO J.* **35**, 1537–1549 (2016).

963 20. Abisambra, J. F. *et al.* DnaJA1 Antagonizes Constitutive Hsp70-Mediated Stabilization of
964 Tau. *J. Mol. Biol.* **421**, 653–661 (2012).

965 21. Thompson, A. D. *et al.* Analysis of the Tau-Associated Proteome Reveals That Exchange of
966 Hsp70 for Hsp90 Is Involved in Tau Degradation. *ACS Chem. Biol.* **7**, 1677–1686 (2012).

967 22. Sarkar, M., Kuret, J. & Lee, G. Two motifs within the tau microtubule-binding domain
968 mediate its association with the hsc70 molecular chaperone. *J Neurosci Res* **86**, 2763–2773
969 (2008).

970 23. Joseph, M., Anglada-Huguet, M., Paesler, K., Mandelkow, E. & Mandelkow, E.-M. Anti-
971 aggregant tau mutant promotes neurogenesis. *Mol Neurodegener* **12**, 88 (2017).

972 24. Pir, G. J. *et al.* Suppressing Tau Aggregation and Toxicity by an Anti-Aggregant Tau
973 Fragment. *Mol Neurobiol* **56**, 3751–3767 (2019).

974 25. Sydow, A. *et al.* Tau-Induced Defects in Synaptic Plasticity, Learning, and Memory Are
975 Reversible in Transgenic Mice after Switching Off the Toxic Tau Mutant. *J Neurosci* **31**, 2511–
976 2525 (2011).

977 26. Mocanu, M.-M. *et al.* The Potential for -Structure in the Repeat Domain of Tau Protein
978 Determines Aggregation, Synaptic Decay, Neuronal Loss, and Coassembly with Endogenous
979 Tau in Inducible Mouse Models of Tauopathy. *J Neurosci* **28**, 737–748 (2008).

980 27. Bergen, M. von *et al.* Mutations of Tau Protein in Frontotemporal Dementia Promote
981 Aggregation of Paired Helical Filaments by Enhancing Local β-Structure. *J Biol Chem* **276**,
982 48165–48174 (2001).

983 28. Smith, E. D. *et al.* Tau from SPAM Transgenic Mice Exhibit Potent Strain-Specific Prion-
984 Like Seeding Properties Characteristic of Human Neurodegenerative Diseases. *NeuroMolecular*
985 *Med.* **27**, 44 (2025).

986 29. Morito, T. *et al.* Human MAPT knockin mouse models of frontotemporal dementia for the
987 neurodegenerative research community. *Cell Rep. Methods* **5**, 101024 (2025).

988 30. Beckman, D. *et al.* A novel tau-based rhesus monkey model of Alzheimer's pathogenesis.
989 *Alzheimer's Dement.* **17**, 933–945 (2021).

990 31. Scheres, S. H., Zhang, W., Falcon, B. & Goedert, M. Cryo-EM structures of tau filaments.
991 *Curr. Opin. Struct. Biol.* **64**, 17–25 (2020).

992 32. Fitzpatrick, A. W. P. *et al.* Cryo-EM structures of tau filaments from Alzheimer's disease.
993 *Nature* **547**, 185–190 (2017).

994 33. Tarutani, A. *et al.* Cryo-EM structures of tau filaments from SH-SY5Y cells seeded with
995 brain extracts from cases of Alzheimer's disease and corticobasal degeneration. *FEBS Open Bio*
996 **13**, 1394–1404 (2023).

997 34. Arakhamia, T. *et al.* Posttranslational Modifications Mediate the Structural Diversity of
998 Tauopathy Strains. *Cell* (2020) doi:10.1016/j.cell.2020.01.027.

999 35. Schweighauser, M. *et al.* Cryo-EM structures of tau filaments from the brains of mice
1000 transgenic for human mutant P301S Tau. *Acta Neuropathol. Commun.* **11**, 160 (2023).

1001 36. Zhao, W. *et al.* Cryo-EM structures reveal variant Tau amyloid fibrils between the rTg4510
1002 mouse model and sporadic human tauopathies. *Cell Discov.* **10**, 27 (2024).

1003 37. Chen, D. *et al.* FTD-tau S320F mutation stabilizes local structure and allosterically promotes
1004 amyloid motif-dependent aggregation. *Nat. Commun.* **14**, 1625 (2023).

1005 38. Nixon, R. A. Autophagy–lysosomal-associated neuronal death in neurodegenerative disease.
1006 *Acta Neuropathol.* **148**, 42 (2024).

1007 39. Ihara, Y., Morishima-Kawashima, M. & Nixon, R. The Ubiquitin–Proteasome System and
1008 the Autophagic–Lysosomal System in Alzheimer Disease. *Cold Spring Harb. Perspect. Med.* **2**,
1009 a006361 (2012).

1010 40. Keller, J. N., Hanni, K. B. & Markesbery, W. R. Impaired Proteasome Function in
1011 Alzheimer's Disease. *J. Neurochem.* **75**, 436–439 (2000).

1012 41. Bobkova, N. V. *et al.* Therapeutic Effect of Exogenous Hsp70 in Mouse Models of
1013 Alzheimer's Disease. *J. Alzheimer's Dis.* **38**, 425–435 (2014).

1014 42. Voss, K., Combs, B., Patterson, K. R., Binder, L. I. & Gamblin, T. C. Hsp70 Alters Tau
1015 Function and Aggregation in an Isoform Specific Manner. *Biochemistry* **51**, 888–898 (2012).

1016 43. Nachman, E. *et al.* Disassembly of Tau fibrils by the human Hsp70 disaggregation machinery
1017 generates small seeding-competent species. *J Biol Chem* **295**, 9676–9690 (2020).

1018 44. Young, Z. T. *et al.* Stabilizing the Hsp70-Tau Complex Promotes Turnover in Models of
1019 Tauopathy. *Cell Chem. Biol.* **23**, 992–1001 (2016).

1020 45. Fontaine, S. N. *et al.* The active Hsc70/tau complex can be exploited to enhance tau turnover
1021 without damaging microtubule dynamics. *Hum Mol Genet* **24**, 3971–3981 (2015).

1022 46. Fontaine, S. N. *et al.* Isoform-selective Genetic Inhibition of Constitutive Cytosolic Hsp70
1023 Activity Promotes Client Tau Degradation Using an Altered Co-chaperone Complement*. *J Biol*
1024 *Chem* **290**, 13115–13127 (2015).

1025 47. Yang, X. & Tohda, C. Heat Shock Cognate 70 Inhibitor, VER-155008, Reduces Memory
1026 Deficits and Axonal Degeneration in a Mouse Model of Alzheimer's Disease. *Front. Pharmacol.*
1027 **9**, 48 (2018).

1028 48. Jinwal, U. K. *et al.* Chemical Manipulation of Hsp70 ATPase Activity Regulates Tau
1029 Stability. *J Neurosci* **29**, 12079–12088 (2009).

1030 49. Yu, A. *et al.* Tau protein aggregates inhibit the protein-folding and vesicular trafficking arms
1031 of the cellular proteostasis network. *J Biol Chem* **294**, 7917–7930 (2019).

1032 50. Dou, F. *et al.* Chaperones increase association of tau protein with microtubules. *Proc*
1033 *National Acad Sci* **100**, 721–726 (2003).

1034 51. Vries, L. E. de *et al.* Gene-expression profiling of individuals resilient to Alzheimer's disease
1035 reveals higher expression of genes related to metallothionein and mitochondrial processes and no
1036 changes in the unfolded protein response. *Acta Neuropathol. Commun.* **12**, 68 (2024).

1037 52. Hondius, D. C. *et al.* The proteome of granulovacuolar degeneration and neurofibrillary
1038 tangles in Alzheimer's disease. *Acta Neuropathol.* **141**, 341–358 (2021).

1039 53. Dickey, C. A. *et al.* The high-affinity HSP90-CHIP complex recognizes and selectively
1040 degrades phosphorylated tau client proteins. *J Clin Invest* **117**, 648–658 (2007).

1041 54. Salminen, A., Ojala, J., Kaarniranta, K., Hiltunen, M. & Soininen, H. Hsp90 regulates tau
1042 pathology through co-chaperone complexes in Alzheimer's disease. *Prog Neurobiol* **93**, 99–110
1043 (2011).

1044 55. Moll, A. *et al.* Hsp multichaperone complex buffers pathologically modified Tau. *Nat*
1045 *Commun* **13**, 3668 (2022).

1046 56. Karagöz, G. E. *et al.* Hsp90-Tau Complex Reveals Molecular Basis for Specificity in
1047 Chaperone Action. *Cell* **156**, 963–974 (2014).

1048 57. Cook, C. *et al.* Loss of HDAC6, a novel CHIP substrate, alleviates abnormal tau
1049 accumulation. *Hum Mol Genet* **21**, 2936–45 (2012).

1050 58. Dickey, C. A. *et al.* Akt and CHIP coregulate tau degradation through coordinated
1051 interactions. *P Natl Acad Sci Usa* **105**, 3622–7 (2008).

1052 59. Weickert, S., Wawrzyniuk, M., John, L. H., Rüdiger, S. G. D. & Drescher, M. The
1053 mechanism of Hsp90-induced oligomerizaton of Tau. *Sci Adv* **6**, eaax6999 (2020).

1054 60. Rutledge, B. S., Choy, W.-Y. & Duennwald, M. L. Folding or holding?—Hsp70 and Hsp90
1055 chaperoning of misfolded proteins in neurodegenerative disease. *J. Biol. Chem.* **298**, 101905
1056 (2022).

1057 61. Jinwal, U. K. *et al.* Imbalance of Hsp70 family variants fosters tau accumulation. *FASEB J.*
1058 **27**, 1450–1459 (2013).

1059 62. Miyata, Y. *et al.* Cysteine Reactivity Distinguishes Redox Sensing by the Heat-Inducible and
1060 Constitutive Forms of Heat Shock Protein 70. *Chem. Biol.* **19**, 1391–1399 (2012).

1061 63. Shelton, L. B. *et al.* Hsp90 activator Aha1 drives production of pathological tau aggregates.
1062 *Proc National Acad Sci* **114**, 9707–9712 (2017).

1063 64. Jinwal, U. K. *et al.* The Hsp90 Cochaperone, FKBP51, Increases Tau Stability and
1064 Polymerizes Microtubules. *J. Neurosci.* **30**, 591–599 (2010).

1065 65. Blair, L. J. *et al.* Accelerated neurodegeneration through chaperone-mediated
1066 oligomerization of tau. *J. Clin. Investig.* **123**, 4158–4169 (2013).

1067 66. Webster, J. M. *et al.* Hsp22 with an N-Terminal Domain Truncation Mediates a Reduction in
1068 Tau Protein Levels. *Int. J. Mol. Sci.* **21**, 5442 (2020).

1069 67. Ospina, S. R. *et al.* Small Heat Shock Protein 22 Improves Cognition and Learning in the
1070 Tauopathic Brain. *Int J Mol Sci* **23**, 851 (2022).

1071 68. Abisambra, J. F. *et al.* Phosphorylation Dynamics Regulate Hsp27-Mediated Rescue of
1072 Neuronal Plasticity Deficits in Tau Transgenic Mice. *J. Neurosci.* **30**, 15374–15382 (2010).

1073 69. Barghorn, S., Biernat, J. & Mandelkow, E. Amyloid Proteins, Methods and Protocols.
1074 *Methods Mol. Biol. (Clifton, NJ)* **299**, 35–51 (2004).

1075 70. Farizatto, K. L. G., Almeida, M. F., Long, R. T. & Bahr, B. A. Early Synaptic Alterations
1076 and Selective Adhesion Signaling in Hippocampal Dendritic Zones Following Organophosphate
1077 Exposure. *Sci. Rep.* **9**, 6532 (2019).

1078 71. Almeida, M. F. *et al.* Distinct and dementia-related synaptopathy in the hippocampus after
1079 military blast exposures. *Brain Pathol.* **31**, e12936 (2021).

1080 72. McKenna, M. *et al.* Organotypic whole hemisphere brain slice models to study the effects of
1081 donor age and oxygen-glucose-deprivation on the extracellular properties of cortical and striatal
1082 tissue. *J. Biol. Eng.* **16**, 14 (2022).

1083 73. Bahr, B. A. *et al.* Amyloid β protein is internalized selectively by hippocampal field CA1 and
1084 causes neurons to accumulate amyloidogenic carboxyterminal fragments of the amyloid
1085 precursor protein. *J. Comp. Neurol.* **397**, 139–147 (1998).

1086 74. Caba, E. *et al.* Excitotoxic stimulation activates distinct pathogenic and protective expression
1087 signatures in the hippocampus. *J. Cell. Mol. Med.* **25**, 9011–9027 (2021).

1088 75. Farizatto, K. L. G., Ikonne, U. S., Almeida, M. F., Ferrari, M. F. R. & Bahr, B. A. Aβ42-
1089 mediated proteasome inhibition and associated tau pathology in hippocampus are governed by a
1090 lysosomal response involving cathepsin B: Evidence for protective crosstalk between protein
1091 clearance pathways. *PLoS ONE* **12**, e0182895 (2017).

1092